Nuclear Engineering and Technology 57 (2025) 103590

Contents lists available at ScienceDirect

Nuclear Engineering and Technology

journal homepage: www.elsevier.com/locate/net

Original Article

Methodology and preliminary verification of generating heterogeneous multigroup microscopic cross-section libraries for neutron transport codes based on OpenMC

Bowen Cui [a,b,*], Guohua Chen [b], Xiaofeng Jiang [b]

[a] Polytechnique Montreal, Station Centre-Ville, Montreal, QC, Canada, H3C3A7
[b] Shanghai NuStar Nuclear Power Technology Co., Ltd., Shanghai, 200240, China

ARTICLE INFO

Keywords:
Monte Carlo
Cross section generation
Multigroup microscopic cross-sections

ABSTRACT

Advancements in reactor technology, particularly Generation IV and modular reactors, have introduced new challenges on the neutronics analysis due to their complex geometries and spectra. This study addresses these challenges by developing a methodology to generate heterogeneous multigroup microscopic cross-section libraries for three-dimensional neutron transport calculations using the OpenMC Monte Carlo code. The approach involves two-dimensional transport calculations in OpenMC for various fuel pins or supercells, generating multigroup microscopic cross-section libraries for isotopes relevant to burnup, temperature, and moderator density. These cross-sections are then post-processed and used in three-dimensional core neutron transport calculations with the CRANE deterministic code. This method combines the high accuracy of Monte Carlo methods with the computational efficiency of deterministic approaches. Preliminary 2D verification was conducted using benchmark problems, including PWR fuel assemblies from the VERA series, a fast reactor pin, a 3600 MWth subassembly, and a 1000 MWth metallic fuel core. Results indicate that the coupled OpenMC/CRANE method accurately captures reactivity and isotopic evolution during burnup, suggesting potential improvements in accuracy and efficiency for neutronic simulations of advanced reactor designs.

1. Introduction

As the global pursuit and enhancement of economic efficiency and safety in the nuclear energy sector continues, the development of nuclear reactors has entered a new era, with Generation IV reactors and modular reactors becoming more sophisticated and diverse, featuring increasingly complex geometries and spectra, which pose additional challenges to neutronic simulation tools. The Monte Carlo (MC) method with point-wise continuous energy cross-sections can address neutron transport problems in complex geometric structures without major approximation in resonance treatment. However, this method demands significant computational resources and time. In comparison, deterministic methods have an advantage in terms of computational resource costs but introduce a series of simplifications and assumptions during the solution process. The applicability of these assumptions varies depending on the reactor type and energy spectrum. For example, in fast reactors with hard spectra, where the average neutron free path is relatively long, accurate treatment of resonance effects requires complex and precise handling, including the use of fine-group treatment, which can impact computational efficiency. Additionally, the new advanced reactors have a variety of fuel forms. The peculiarities of the pebble bed reactor structure introduce challenges due to the presence of double heterogeneity.

Some Monte Carlo programs have incorporated the capability to generate group constants for coupling with downstream core programs. Fridman and Leppänen investigated the use of the Serpent code for generating homogeneous cross sections [1]. Park et al. also developed McCARD as a few-group constant generator [2], while Hoogenboom et al. developed MCNP5 for the generation of multi-group cross sections and scattering matrices [3]. In the latest version, OpenMC [4] provides a tally system that allows for the calculation of multi-group cross sections with arbitrary energy discretizations. Furthermore, a new function, openmc.deplete.get_microxs_and_flux (), was introduced in OpenMC (v0.14.0) to generate microscopic cross sections along with fluxes, thereby making multi-group cross section generation and depletion analysis more convenient.

* Corresponding author. Polytechnique Montreal, Station Centre-Ville, Montreal QC, H3C3A7, Canada.
E-mail address: bowen.cui@polymtl.ca (B. Cui).

https://doi.org/10.1016/j.net.2025.103590
Received 2 December 2024; Received in revised form 9 March 2025; Accepted 17 March 2025
Available online 19 March 2025
1738-5733/© 2025 Korean Nuclear Society, Published by Elsevier Korea LLC. All rights are reserved, including those for text and data mining, AI training, and similar technologies. This is an open access article under the CC BY-NC-ND license (http://creativecommons.org/licenses/by-nc-nd/4.0/).

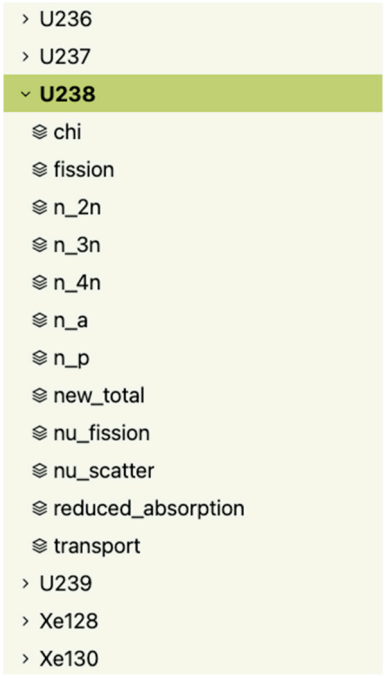


Fig. 1. Microscopic cross sections of various nuclides stored in the HDF5 format.

The development of Monte Carlo codes has led to an increasing focus on hybrid methods that combine MC solvers with deterministic strategies, aiming to leverage the advantages of both Monte Carlo and deterministic approaches. Two-step schemes that couple multigroup cross-sections (MGXS) with diffusion core solvers have been extensively studied. Examples include Serpent/RAST [5], Serpent/VARIANT [6,7], OpenMC/OpenMC [8], MCS/RAST [9] for fast reactors, MCS/PARCS for pressurized water reactors [10], Shift/Griffin for heat pipe reactors[11], and OpenMC/VSOP for very high-temperature reactors [12].

The aforementioned methods are based on macroscopic cross-

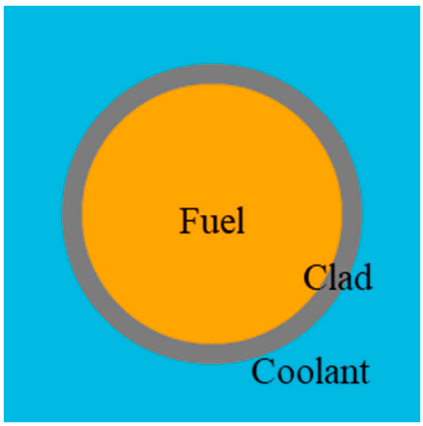


Fig. 3. Simplified single pin-cell model of fuel.

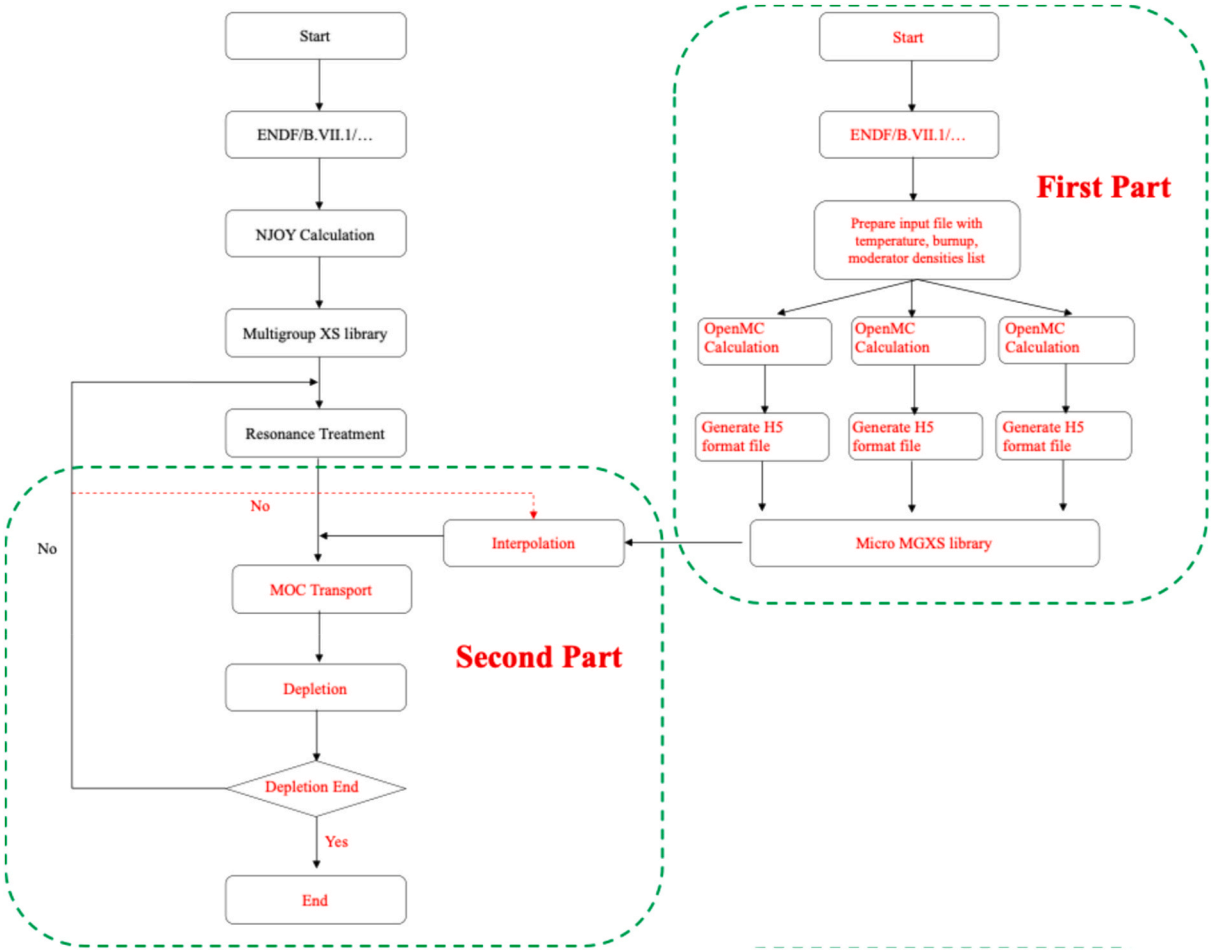


Fig. 2. Overall coupled calculation process and microscopic cross-section library generation steps.

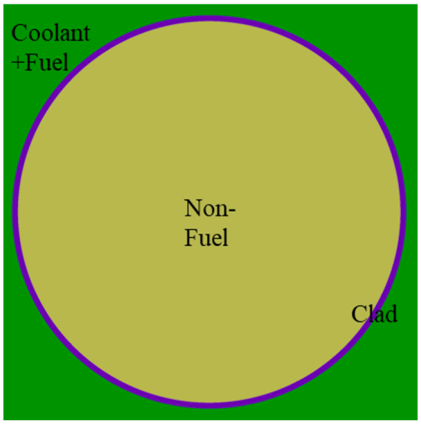


Fig. 4. Simplified single pin-cell model of non-fuel.

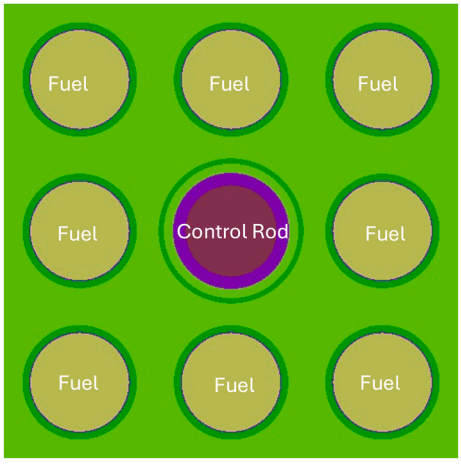


Fig. 5. Nine-grid super-cell model.

sections, which require considering various material-related physical parameters. This approach also involves spatial homogenization and the issue of equivalent homogenization, which necessitates the use of SPH factors (in downstream transport codes) or discontinuity factors (in downstream diffusion codes). These factors not only affect the accuracy but also increase the complexity of the program. However, this study aims to explore a direct coupling method that utilizes microscopic cross-sections in Monte Carlo-lattice transport calculations. By employing a multigroup, heterogeneous, and microscopic cross-section model that accounts for variations in fuel burnup rates and nuclide compositions resulting from different power histories, the power history effects and energy spectrum interference between fuel assemblies can be more accurately captured. This approach has better generality, especially for thermal reactors with graphite as a moderator, where the neutron mean free path is long, as well as for fast neutron reactors.

Nonetheless, as [13,14] have pointed out, even when using heterogeneous multi-group microscopic cross-section libraries, equivalence parameters (such as SPH factors) are still necessary to correct condensation errors resulting from the neglect of angle dependency in total cross sections and cross-section discretization. These errors are particularly significant for thermal neutron reactors. In practical simulations, increasing the number of energy groups can reduce errors caused by angle dependency and group condensation; however, this significantly raises computational complexity and memory requirements. In this study, we utilize a high-performance one-step method with a moderate number of energy groups (e.g., 33 groups) to address the multi-group problem and observe how this choice affects the accuracy and potential biases in power distribution.

To achieve this goal, a method is proposed for generating heterogeneous multi-group microscopic cross-section libraries for three-dimensional neutron transport calculations using OpenMC. The approach involves performing two-dimensional transport calculations in OpenMC for various types of fuel pins or supercells, and then generating multi-group microscopic cross-section tables for isotopes related to burnup, temperature, and density for three-dimensional core neutron transport calculations. In this work, an automated process for generating multi-group microscopic cross-section libraries and coupling interface with the three-dimensional neutron transport code was developed. The primary objective of this study is to combine the respective strengths of OpenMC and the high-performance full-core transport software CRANE to establish a computational framework with strong adaptability to various reactor types. This framework enables rapid and reliable analysis for different advanced reactor designs.

However, the current work remains preliminary, and further detailed studies will be conducted in the future, such as the selection of supercell models, the energy group structure, and the number of groups suitable for reactors with different spectra. As a first step toward validating the

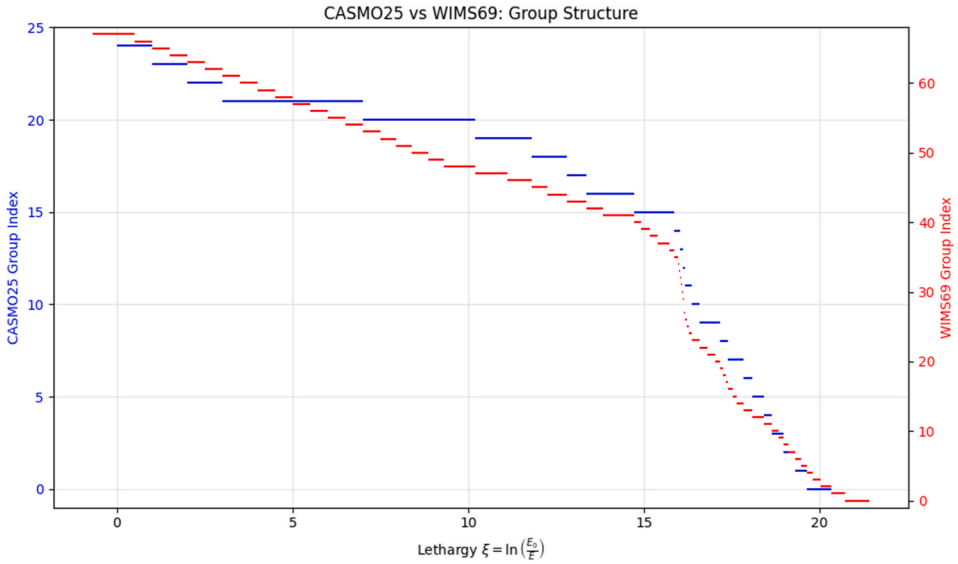


Fig. 6. Comparison of lethargy width between CASMO 25 group and WIMS 69 group structures.

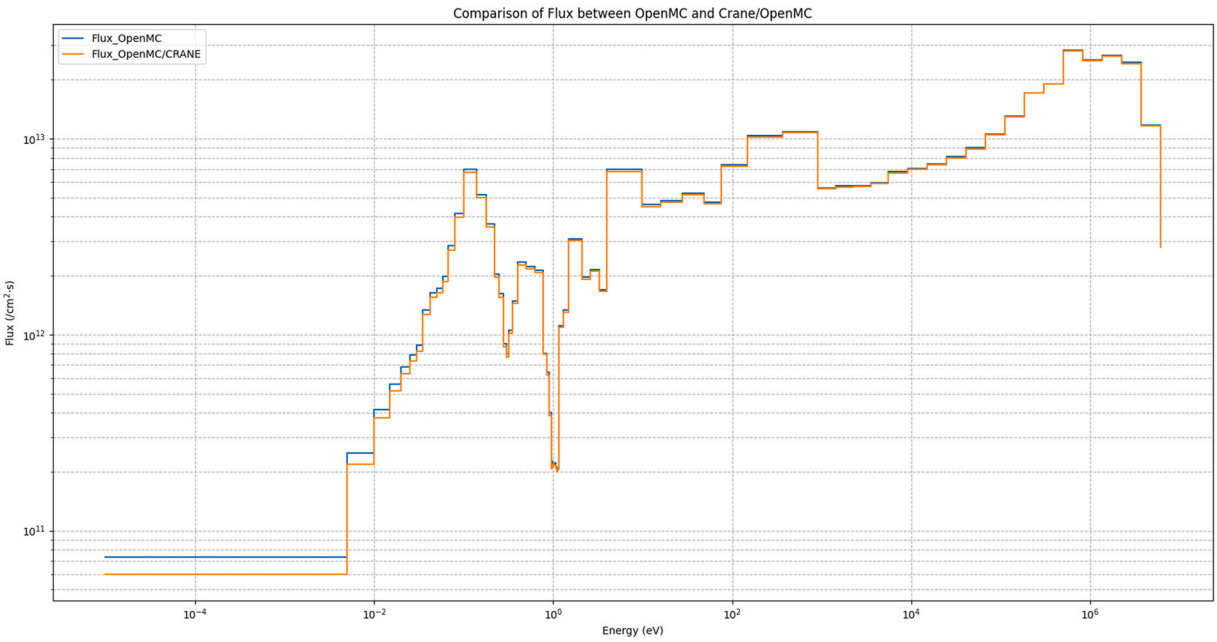


Fig. 7. Neutron spectrum of VERA 1B OpenMC and OpenMC/CRANE.

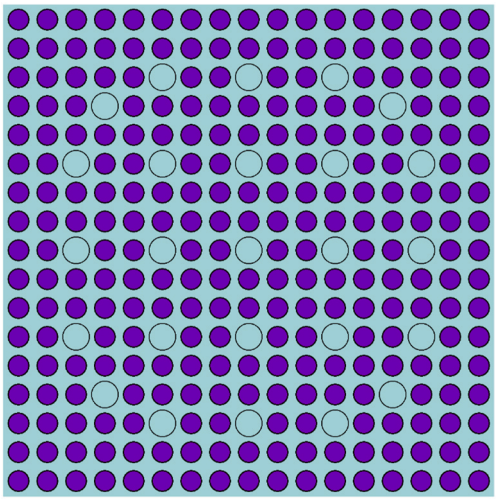


Fig. 8. Vera 2A&2C assembly Configuration.

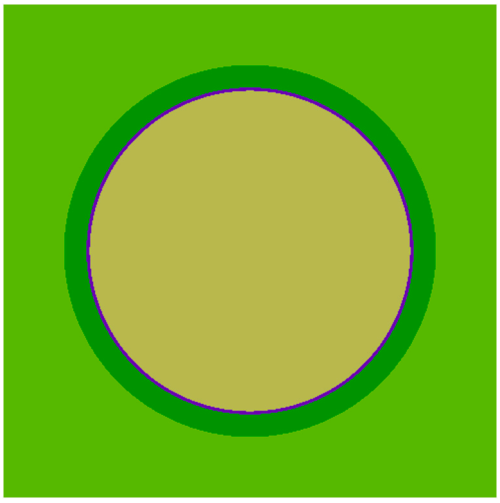


Fig. 9. VERA Pin geometry.

feasibility of this methodology, preliminary two-dimensional verification was conducted using benchmark problems, including pressurized water reactor (PWR) single pins, fuel assemblies from the VERA series, a fast reactor pin, a 3600 MWth subassembly, and a 1000 MWth metallic fuel core. While this study focuses on two-dimensional verification, the developed methodology and tools are directly applicable to three-dimensional transport simulations. Extending this framework to three-dimensional verification is planned as a future step under the same computational approach.

The paper structure is the following.

- in section 2, computer codes used in this study are briefly introduced.
- Section 3 describes the necessary theory and the calculation schemes.
- Section 4 discusses the verification results.
- Section 5 concludes the study and discusses future perspectives.

Table 1
OpenMC/CRANE results for the pin-cell problem.

	OpenMC K_{eff}	OpenMC/CRANE K_{eff}	diff (pcm)
VERA 1B pin	1.1839	1.1819	−168.9

- Appendix provides detailed models and parameters used for generating multigroup microscopic cross-section libraries for fast reactor core calculation

2. Computer codes

This section provides an introduction to the computer code used in this study. The Monte Carlo code OpenMC is utilized for generating microscopic cross-section libraries, which are then provided to the lattice neutron deterministic transport code CRANE.

Table 2
Time-steps used for 2D fuel assembly depletion calculations.

	Burn up (GWd/tHM)
OpenMC fuel single pin-cell model used to generate microscopic XS	0.0, 0.01, 0.25, 0.5, 4, 12, 20, 30, 40, 50, 60
OpenMC reference assembly calculation	0, 0.01, 0.25, 0.5, 1, 2, 3, 4, 5, 6, 7, 8, 9, 10, 11, 12, 13, 14, 15, 16, 17, 18, 19, 20, 22.5, 25, 27.5, 30, 32.5, 35, 37.5, 40, 42.5, 45, 47.5, 50, 52.5, 55, 57.5, 60
OpenMC/CRANE assembly calculation	0, 0.01, 0.25, 0.5, 1, 2, 3, 4, 5, 6, 7, 8, 9, 10, 11, 12, 13, 14, 15, 16, 17, 18, 19, 20, 22.5, 25, 27.5, 30, 32.5, 35, 37.5, 40, 42.5, 45, 47.5, 50, 52.5, 55, 57.5, 60

2.1. OpenMC

OpenMC [15] is a community-developed Monte Carlo neutron and photon transport code. OpenMC was originally developed by members of the Computational Reactor Physics Group at the Massachusetts Institute of Technology starting in 2011. It is capable of performing fixed source, k-eigenvalue, and subcritical multiplication calculations. A flexible and efficient tally system enables a wide variety of physical quantities to be tallied and analyzed. In this study, the v0.13.2 version of OpenMC was utilized with minimal modifications to the source code. The calculations were performed using the ENDF/B-VII.1 cross-section database and the Simplified Chain (Thermal and Fast Spectrum) depletion chain [16].

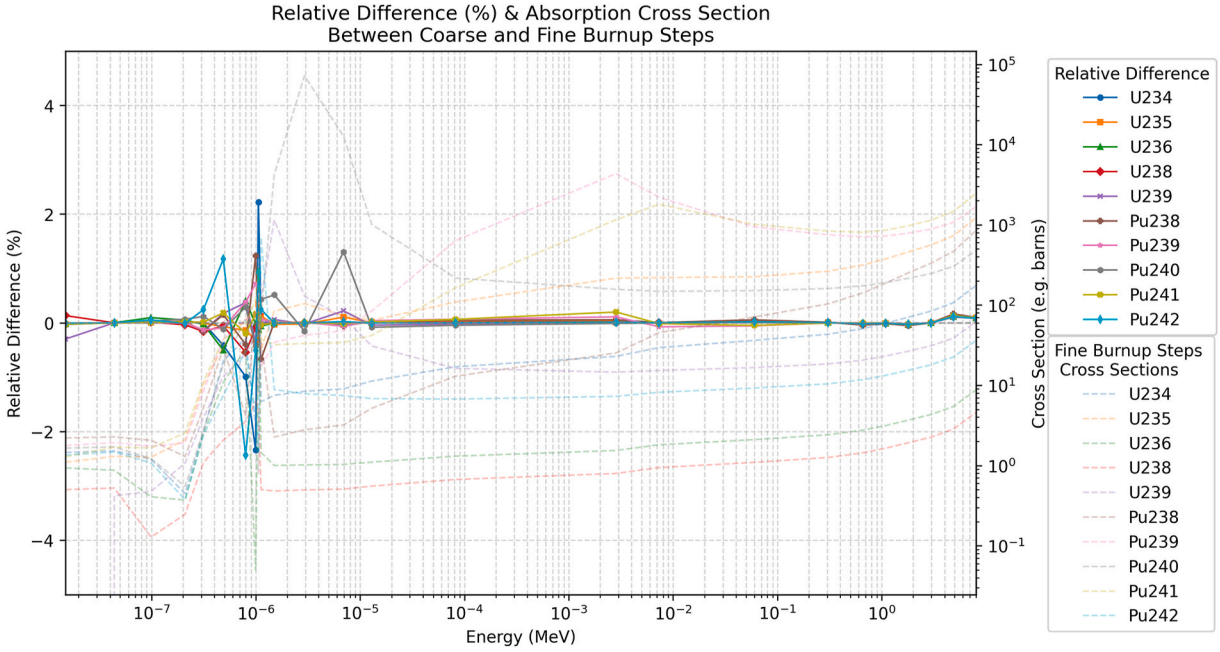


Fig. 10. Relative difference (%) of absorption cross section between coarse and fine burnup steps.

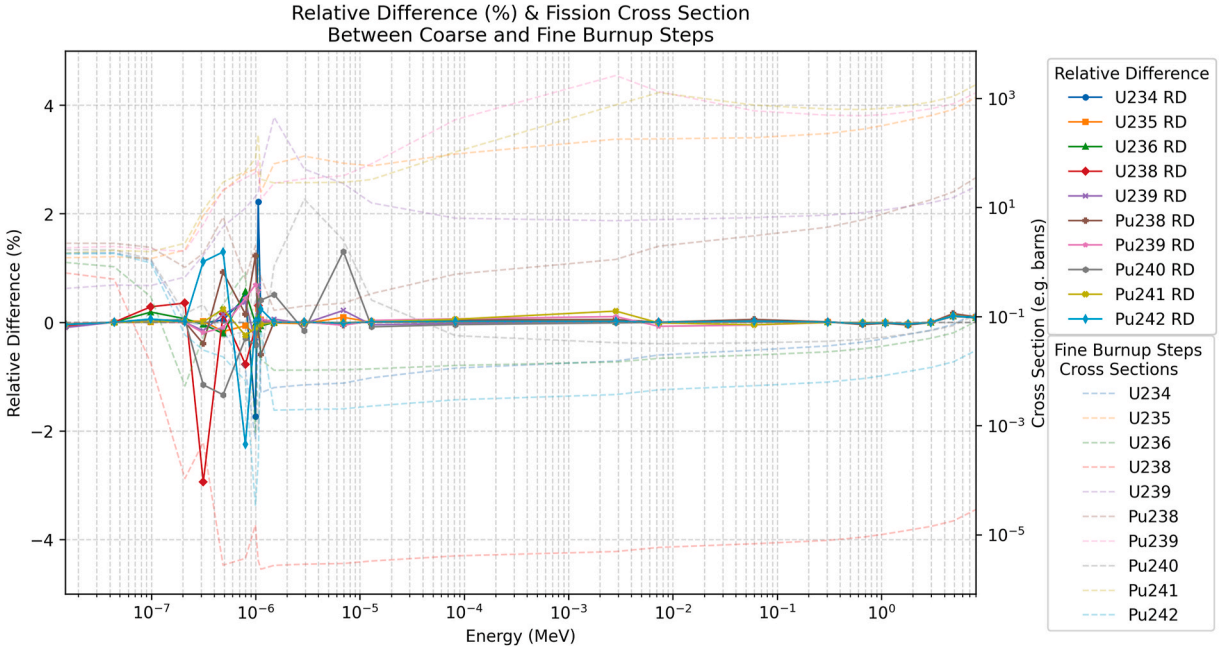


Fig. 11. Relative difference (%) of fission cross section between coarse and fine burnup steps.

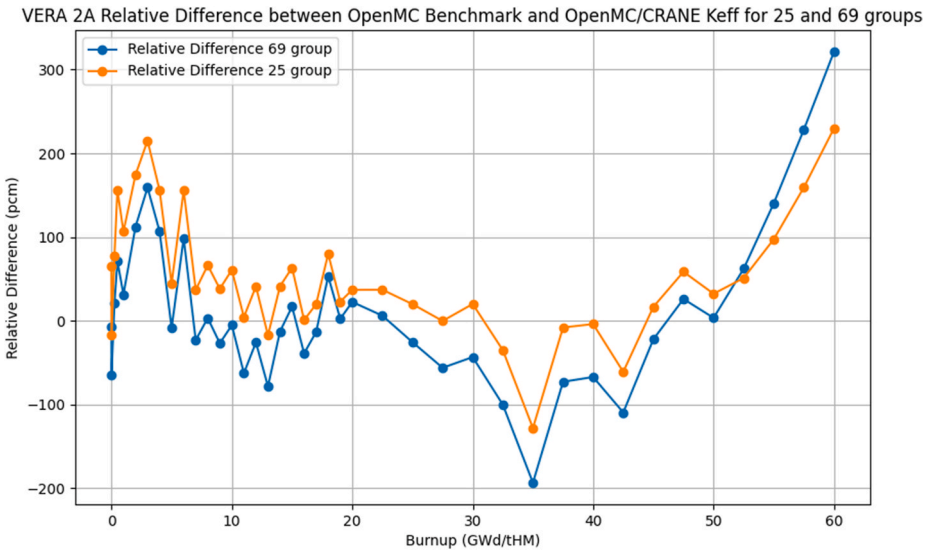


Fig. 12. VERA 2A: K_{eff} Relative Difference between OpenMC Benchmark and OpenMC/CRANE for 25 and 69 groups.

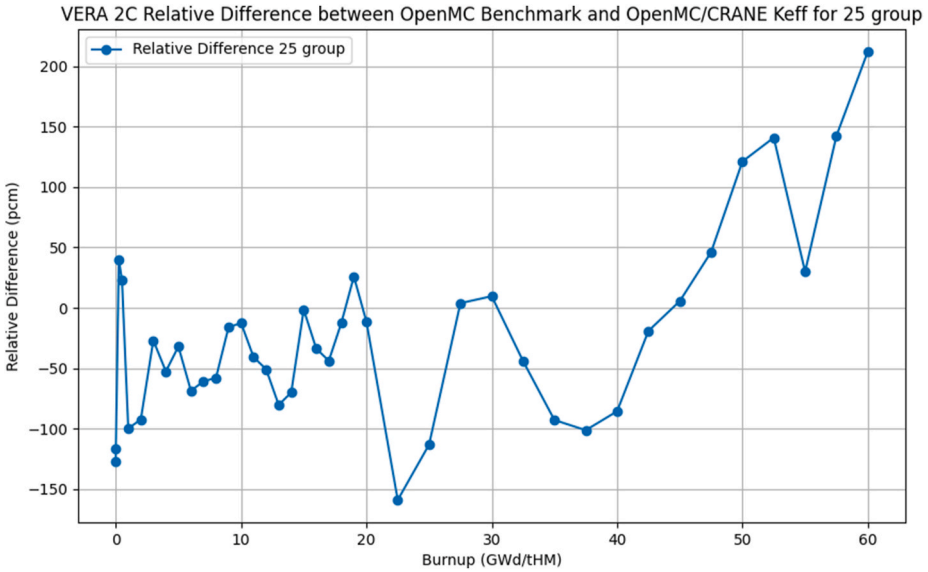


Fig. 13. Vera 2C: Relative difference between OpenMC benchmark and OpenMC/CRANE K_{eff}

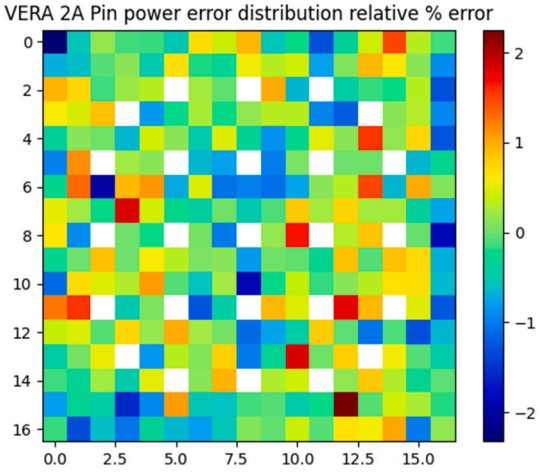


Fig. 14. Vera 2A: 60GWd/tHM pin power error distribution relative % error.

2.2. CRANE

CRANE [17], developed by Shanghai NuStar Nuclear Power Technology Co., Ltd., is a coupled neutronics/thermal-hydraulics analysis code based on CPU-GPU heterogeneous platforms. CRANE performs fine-grained three-dimensional core calculations at the pin-by-pin level, based on the Method of Characteristics (MOC) for solving the neutron transport equation. The code integrates the solution of the three-dimensional neutron transport equation, the nuclide burnup equation, the subchannel thermal-hydraulic equations, and the fuel performance analysis. This allows for the direct determination of various physical parameters inside the reactor, such as neutron flux distribution, temperature distribution, and nuclide composition distribution, based on a detailed modeling of the real reactor core. The code also provides visualization of these parameters. Currently, CRANE has been validated and confirmed for more than 150 reactor-years for different pressurized water reactor designs. Compared to the traditional two-step nuclear design software, CRANE has a significant advantage in terms of calculation accuracy. CRANE demonstrates excellent computational

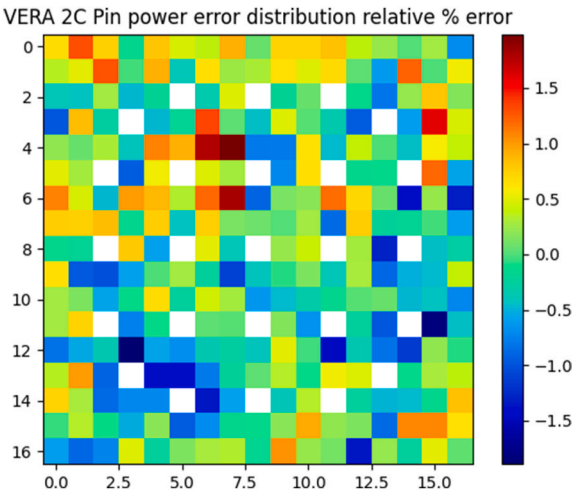


Fig. 15. Vera 2C: 60GWd/tHM pin power error distribution relative % error.

performance, utilizing CUDA for GPU parallel acceleration, and can achieve an average of 30 s per state point for million to ten-million-node commercial pressurized water reactor 1/4-core tracking simulations on a server equipped with 10 RTX4090 graphics cards. Shanghai Nuclear Star Nuclear Power Technology Co., Ltd. has developed an interface that seamlessly converts computational models from OpenMC into CRANE models with a single click. Since both CRANE and OpenMC utilize the Constructive Solid Geometry (CSG) approach for radial modeling, this ensures full compatibility and a smooth transition between the two codes. With this conversion interface, various fuel assembly and super assembly models for OpenMC can be automatically generated from the three-dimensional core model defined in CRANE. This simplifies the entire process and makes it more user-friendly.

3. Methodology and numerical method

3.1. Microscopic multigroup cross-sections generation

3.1.1. Generation of MGXS by OpenMC

The generation of MGXS by OpenMC [4] is based on tallies with specific scores and filters. Generally, a tally estimator for reaction rate integration of reaction type x over a given volume V can be represented as:

$$\langle \Sigma_x, \psi \rangle_g = \int_V \int_S \int_{E_g}^{E_{g-1}} \Sigma_x(\mathbf{r}, E)\psi(\mathbf{r}, E, \Omega) dE d\Omega d\mathbf{r} \tag{1}$$

where.

$\langle \cdot, \cdot \rangle$: inner products in phase-space (incoming and/or outgoing energy, space and angle)
Σ_x: macroscopic cross sections of reaction type x;
ψ: angular neutron flux;
V: integration bounds in space r;
S: integration bounds in solid angle Ω;
E: integration bounds in energy E;
E_g and E_{g-1}: lower and upper integration bounds in energy group g.

The tally for scalar flux (represented by symbol φ) integration over a given volume V is represented as $\langle \psi \rangle$. The inner product of a function with unity, is denoted by Equation (2):

$$\langle \psi \rangle_g \equiv \langle \psi, 1 \rangle_g = \int_V \int_{4\pi} \int_{E_g}^{E_{g-1}} \psi(\mathbf{r}, E, \Omega) dE d\Omega d\mathbf{r} \tag{2}$$

The general spatially homogenized (over volume V) macroscopic MGXS for reaction x and energy group g can be computed as Equation (3):

$$\Sigma_{x,g} = \frac{\langle \Sigma_x, \psi \rangle_g}{\langle \psi \rangle_g} \tag{3}$$

The general reaction cross-sections, including absorption, fission, and total reaction cross-sections, can be calculated using the track-length estimator based on the provided information. By dividing these cross-sections by the number density of the nuclide, it becomes straightforward to calculate the microscopic form of each MGXS for every nuclide. The fission spectrum depends on the outgoing neutron energy and must be computed using an analog estimator. The calculation can be performed using Equation (4):

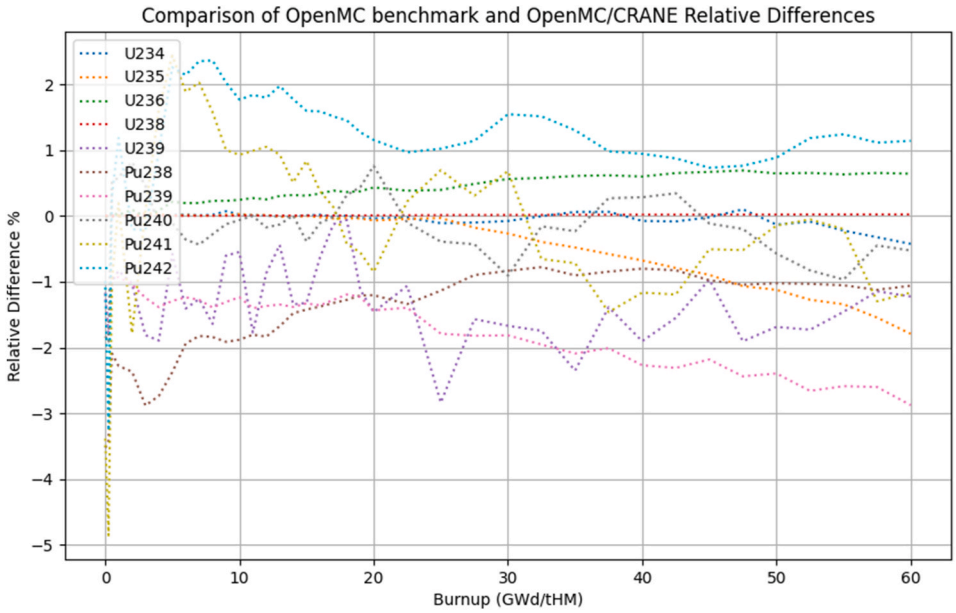


Fig. 16. Vera 2A: Comparison of OpenMC benchmark and OpenMC/CRANE relative differences for 25 groups.

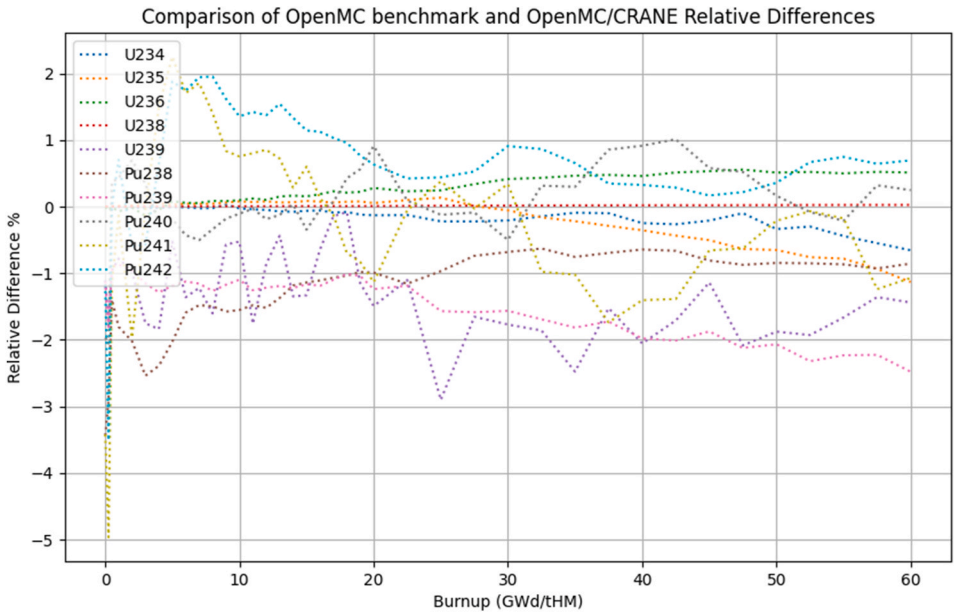


Fig. 17. Vera 2A: Comparison of OpenMC benchmark and OpenMC/CRANE relative differences for 69 groups.

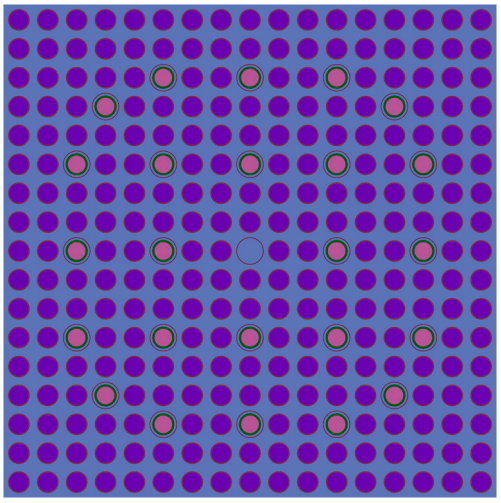


Fig. 18. Vera 2G assembly Configuration.

$$\widehat{\chi}_{k,g} = \frac{\sum_{g'=1}^{G} \langle \nu\Sigma_f, \psi \rangle_{k,g'\to g}}{\sum_{g=1}^{G}\sum_{g'=1}^{G} \langle \nu\Sigma_f, \psi \rangle_{k,g'\to g}} \tag{4}$$

The transport-corrected total cross-sections and scattering cross-sections have distinct characteristics compared to other cross-sections. The previous equation discretized only the energy of the incoming neutrons, disregarding the energy of the outgoing neutrons (if present). By summing the first Legendre scattering moments over all incoming energy groups, the in-scatter approximation can be used to compute the transport-corrected scattering (5). It is important to note that the scattering matrix depends on the outgoing neutron energy, requiring the use of analog estimators. The scattering matrix for the l-th Legendre moment is given by (6). The transport correction is then subtracted from the groupwise total collision rate and normalized by the flux to compute the transport-corrected total cross section (7).

$$\Delta\widehat{\Sigma}_{tr,k,g} = \sum_{g'=1}^{G} \langle \Sigma_{s1}, \psi \rangle_{k,g'\to g} \tag{5}$$

$$\widehat{\Sigma}_{s\ell,k,g'\to g} = \frac{\langle \Sigma_{s\ell}, \psi \rangle_{k,g'\to g}}{\langle \psi \rangle_{k,g'}} \tag{6}$$

$$\widehat{\Sigma}_{tr,k,g} = \frac{\langle \Sigma_t, \psi \rangle_{k,g} - \Delta\widehat{\Sigma}_{tr,k,g}}{\langle \psi \rangle_{k,g}} \tag{7}$$

Once a simulation is finished, an HDF5 state point file is created, which stores the tally results. By using the Python API, the StatePoint object can read and access the tally results from the state point file. This allows for the extraction and output of the multigroup microscopic cross-sections.

3.1.2. *Cross section requirements for fine-mesh deterministic neutron transport code*

The output of OpenMC only includes flux and reaction rate values, and the directly computed multigroup homogenized cross-sections do not consider neutron multiplication effects. To consider (n,xn) reactions, the multigroup neutron transport equation can be rewritten in the following form:

$$\begin{aligned} &\Omega\cdot\nabla\phi_g + \Sigma_{t,g}\phi_g \\ &= \sum_{h=1}^{G}\sum_{n1n}^{h\to g}\phi_h + 2\sum_{h=1}^{G}\sum_{n2n}^{h\to g}\phi_h + 3\sum_{h=1}^{G}\sum_{n3n}^{h\to g}\phi_h + \frac{\chi_g}{k_{\text{eff}}}\sum_{h=1}^{G}\nu\sum_{f,h}\phi_h \end{aligned} \tag{8}$$

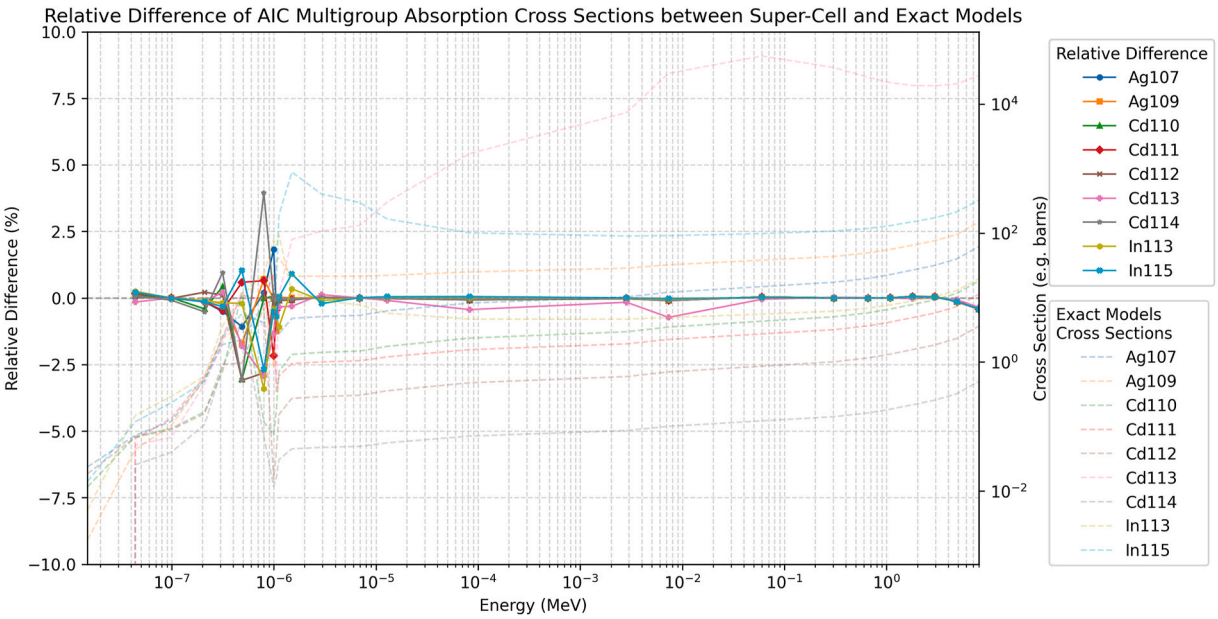


Fig. 19. Relative difference of AIC multigroup absorption cross sections between super-cell and exact models.

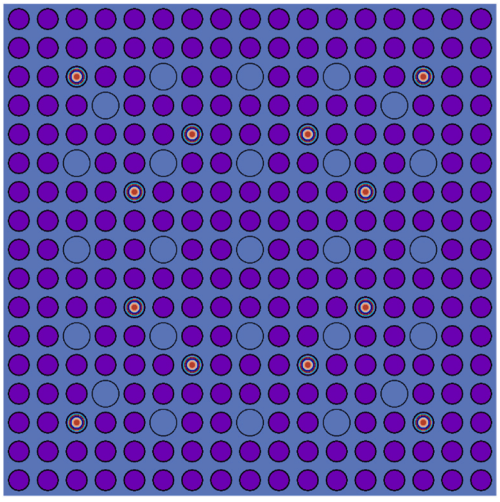


Fig. 20. Vera 2O assembly Configuration.

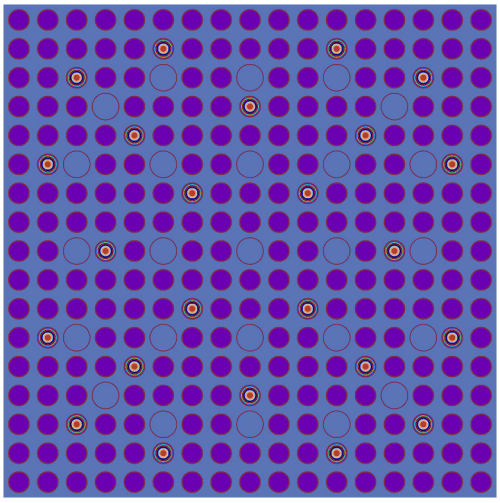


Fig. 21. Vera 2P assembly Configuration.

$$\Omega\cdot\nabla\phi_g + \Sigma_{t,g}\phi_g = \sum_{h=1}^{G}\Sigma_s^{(h\to g)}\phi_h + 2\sum_{h=1}^{G}\Sigma_{(n,2n)}^{(h\to g)}\phi_h + 3\sum_{h=1}^{G}\Sigma_{(n,3n)}^{(h\to g)}\phi_h + 4\sum_{h=1}^{G}\Sigma_{(n,4n)}^{(h\to g)}\phi_h + \frac{\chi_g}{k_{\text{eff}}}\nu\sum_{h=1}^{G}\sum_f \Sigma_f^{(h)}\phi_h \tag{8}$$

$$\Sigma_{t,g} = \Sigma_{a,g} + \Sigma_{n1n,g} + \Sigma_{n2n,g} + \Sigma_{n3n,g} + \Sigma_{n4n,g} \tag{9}$$

$$\Sigma_{a,g} = \Sigma_{\gamma,g} + \Sigma_{(n,p),g} + \Sigma_{(n,\alpha),g} + \cdots\cdots \tag{10}$$

In the equation, g and h represent the energy group indices. The total cross-section $\Sigma_{t,g}$ and absorption cross-section $\Sigma_{a,g}$ are directly obtained from OpenMC. $\Sigma_{n1n,g}$ represents the scattering cross-section used in the calculations, while $\Sigma_{n2n,g}$, $\Sigma_{n3n,g}$, and $\Sigma_{n4n,g}$ represent the $(n,2n)$, $(n,3n)$, and $(n,4n)$ reaction cross-sections, respectively.

For convenience in calculations, we can define an equivalent group total scattering cross-section (11), scattering matrix (12), and absorption cross-section (13):

$$\widetilde{\Sigma}_{s,g} \equiv \Sigma_{n1n,g} + 2\Sigma_{n2n,g} + 3\Sigma_{n3n,g} + 4\Sigma_{n4n,g} \tag{11}$$

$$\widetilde{\Sigma}_s^{h\to g} \equiv \Sigma_{n1n}^{h\to g} + 2\Sigma_{n2n}^{h\to g} + 3\Sigma_{n3n}^{h\to g} + 4\Sigma_{n4n}^{h\to g} \tag{12}$$

$$\widetilde{\Sigma}_{a,g} \equiv \Sigma_{a,g} - \Sigma_{n2n,g} - 2\Sigma_{n3n,g} - 3\Sigma_{n4n,g} \tag{13}$$

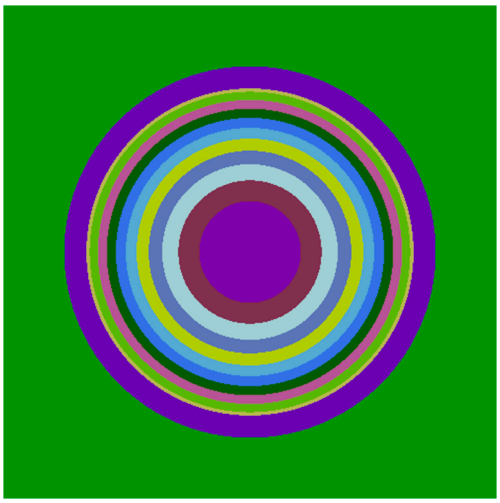


Fig. 22. Gadolinium pin geometry.

This leads us to the neutron transport equation we solve (14) and the redefined total cross-section (15):

$$\Omega \cdot \nabla \phi_g + \left(\widetilde{\Sigma}_{a,g} + \widetilde{\Sigma}_{s,g}\right)\phi_g = \sum_{h=1}^{G} \widetilde{\Sigma}_s^{h\to g}\phi_h + \frac{\chi_g}{k_{\text{eff}}} \sum_{h=1}^{G} \nu\Sigma_{\text{f},h}\phi_h \tag{14}$$

$$\widetilde{\Sigma}_{\text{t},g} = \widetilde{\Sigma}_{a,g} + \widetilde{\Sigma}_{s,g} \tag{15}$$

$$\Sigma_{\text{tr},g} = \Sigma_{\text{t},g} - \mu\Sigma_{\text{s},g} \tag{16}$$

$$\widetilde{\Sigma}_{\text{tr},g} = \widetilde{\Sigma}_{\text{t},g} - \mu\Sigma_{\text{s},g} \tag{17}$$

$$\widehat{\Sigma}_s^{g\to g} \equiv \widetilde{\Sigma}_s^{g\to g} - \mu\Sigma_{s,g} \tag{18}$$

Next, we will edit the transport correction cross-sections. As mentioned earlier, OpenMC is capable of generating transport correction cross-sections using an in-scatter model. Therefore, based on (16), we can calculate the P1 scattering term, $\mu\Sigma_{s,g}$, and then utilize the computed $\widetilde{\Sigma}_{t,g}$ from (15) to recalculate $\widetilde{\Sigma}_{tr,g}$ using (17). Finally, the self-scattering cross-section is corrected based on equation (18).

The Fig. 1 shows the microscopic cross sections of various nuclides stored in the hdf5 format multigroup library.

3.2. Calculation method and model

3.2.1. Overall coupling calculation schema

The overall coupled calculation process and the steps for generating a microscopic cross-section library are illustrated in Fig. 2. The black portion represents the computational flow of the deterministic code CRANE, while the red color represents the two-stage approach OpenMC/CRANE adopted in this study. The figure clearly indicates that the left dataflow corresponds to CRANE, and the right dataflow corresponds to OpenMC.

In CRANE, the primary computational process starts with reading the ENDF/B.VII.1 and JEFF3.3 nuclear evaluation databases. These databases are processed using NJOY2016 [18] to generate a multigroup database. Subsequently, resonance calculations and transport calculations are performed using the energy group structure from the multigroup database. This process is iterated for each burnup step.

The two-stage approach OpenMC/CRANE consists of two parts. In the first part, the objective is to create comprehensive and reliable multigroup microscopic cross-section libraries. The ENDF/B.VII.1 [19] and JEFF3.3 [20] nuclear evaluation databases are read and processed into ACE format using NJOY2016. OpenMC is used to perform neutron transport and depletion calculation for different types of single pin and supercell, then perform branching calculations at different fuel temperatures and moderator densities. The MGXS module is employed to obtain a multigroup microscopic cross-section library. The resulting cross-sections are post-processed according to the cross-section requirements for fine-mesh deterministic neutron transport code, resulting in the final microscopic cross-section library in HDF5 format. In the second part, the coupled calculation with CRANE is performed for the whole core. The cross-section libraries are interpolated based on the computational model, and the resonance calculation is bypassed. The calculation entails using the method of characteristics (MOC) transport and burnup calculations. The interpolation is performed again in each burnup step within a loop.

3.2.2. Consideration of non-lattice effects

Under conditions of given burnup and temperature, effective resonance cross sections in resonance energy groups are primarily influenced by surrounding moderation conditions. Thus, for handling resonance nuclides in resonance energy groups under non-lattice effects, the proposed approach is as follows.

1. In a preliminary calculation using a single unit-cell (or single pin-cell) model, the moderator density is systematically varied under different burnup states to calculate effective resonance cross sections. Concurrently, the Dancoff factor for each moderator density condition is evaluated using the Enhanced Neutron Current Method (ENCM) [21]. The ENCM approach calculates the Dancoff factor via a single-group fixed-source transport calculation. This step establishes a direct relationship between moderator density and the corresponding Dancoff factor.
2. During the full-core calculation, the ENCM is again utilized to determine the Dancoff factor for each fuel pin or region within the core.
3. Based on the Dancoff factor obtained from the full-core calculation, interpolation is performed within the previously established relationship to deduce the corresponding moderator density. This moderator density is then used to interpolate the effective resonance cross sections for subsequent full-core neutron transport calculations.

The effectiveness and accuracy of this procedure in capturing non-lattice effects and resonance self-shielding will be rigorously validated through further numerical studies.

3.2.3. Parametrized microscopic cross-section generation

Generating a parameterized microscopic cross section library requires covering all fuel types, burnup and operating conditions within the reactor core. This necessitates hundreds or thousands of simulations. To save computational time, this study utilizes OpenMC to model and simulate a single pin or super cell problem. For fuel cells with various enrichments, a simplified two-dimensional single-pin fuel-cladding-moderator model with reflective boundary conditions (as shown in Fig. 3) is employed. To capture resonance effects in non-fuel regions (e.g., control rods, reflectors, and shielding), one approach is to employ a two-dimensional equivalent model in which the fuel and moderator are homogenized and uniformly surrounded by a specified thickness of non-fuel material (see Fig. 4). This approach, while sufficient for fast reactor analyses, provides only a crude treatment of spatial self-shielding—especially when resonances in the non-fuel region overlap with those of the fuel region. For thermal reactors, such simplifications are inadequate. Instead, a super-cell model in a nine-grid configuration is chosen, where, for instance, the control rod is positioned at the center, surrounded by eight fuel rods, as depicted in Fig. 5. A detailed verification of this super-cell approach is provided in the following chapter.

The two-stage approach of OpenMC/CRANE allows for the generation of a multigroup microscopic cross-section library with any desired

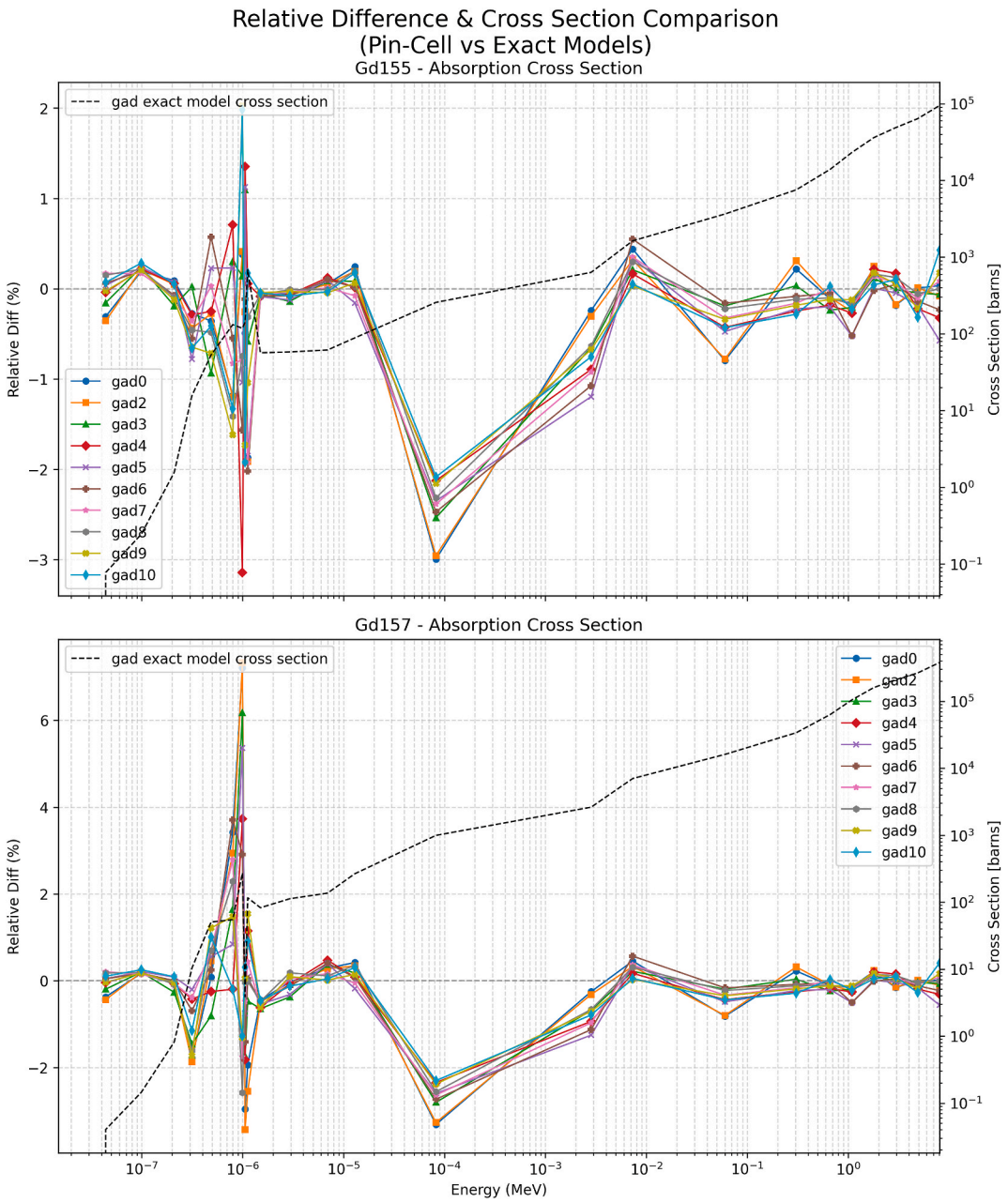


Fig. 23. Comparison of absorption cross sections for Gd-155 and Gd-157 at the final burnup step between the single-pin model and the exact assembly-level configuration.

energy group structure, which can then be used for deterministic whole-core calculations. To balance computational efficiency and accuracy, a 33-group energy structure [22] is chosen for fast reactors in the single pin calculations without major approximations. For pressurized water reactors, either a 69-group structure from WIMS [23] or a 25-group structure from CASMO [24] is selected. Fig. 6 compares the lethargy widths of the CASMO 25-group and WIMS 69-group structures.

When generating a parameterized library, it is necessary to accurately describe resonance phenomena by considering the effects of different moderator densities, burnups, and temperatures on the physical factors in Monte Carlo pin-cell calculations. Performing three-dimensional tabulation requires a significant amount of computational time. To save computation time, all nuclides are categorized into four types: resonant and burnable, non-resonant but burnable, resonant but unburnable, and non-resonant and unburnable materials. For all nuclides, temperature variations need to be considered. In the cross-section tables, temperature intervals such as 100K–200K are selected. In the case of resonant nuclides, in addition to their own temperature, the impact of the surrounding environment (e.g., moderator, coolant temperature, and density) on the resonance self-shielding effect must be taken into account. As for resonant burnable nuclides, burnup effects on resonance self-shielding and mutual shielding need to be considered. Since the effective microscopic cross-sections of resonance energy groups change relatively slowly with burnup, larger burnup steps can be used in the OpenMC burnup simulations when generating the cross-section tables. The use of predictive corrections or other burnup strategies is unnecessary, which can improve the efficiency of producing the cross-section library.

After completing the tabulation, the library is read in CRANE, and in this study, linear interpolation and square root interpolation are chosen. It is found that both interpolation methods have a minor impact on the computed results.

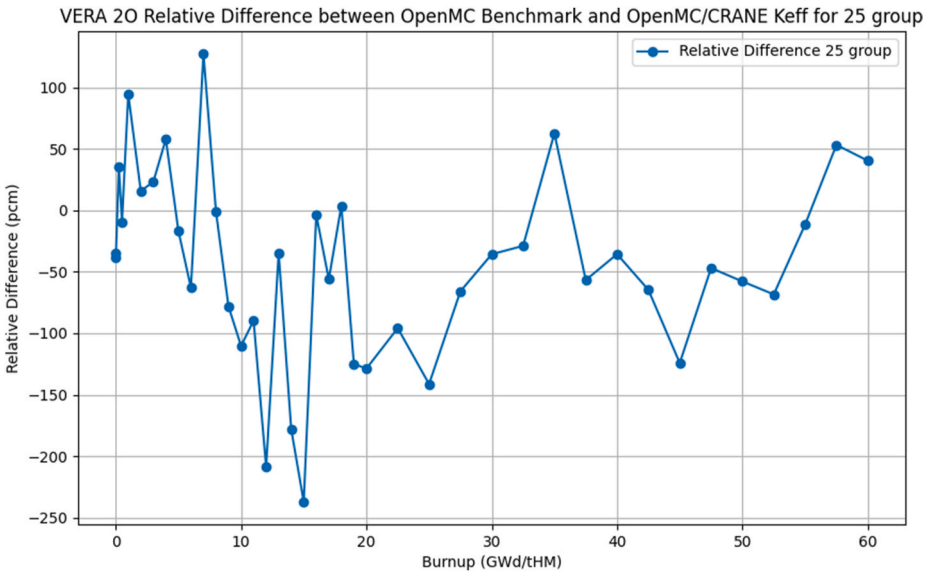


Fig. 24. VERA 2O Relative Difference between OpenMC Benchmark and OpenMC/CRANE K_{eff} for 25 group.

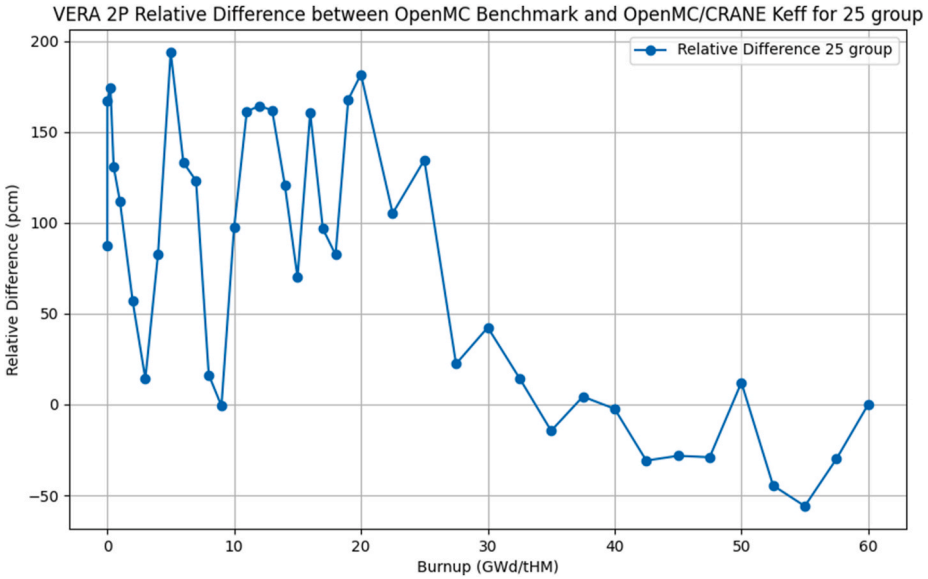


Fig. 25. VERA 2P Relative Difference between OpenMC Benchmark and OpenMC/CRANE K_{eff} for 25 group.

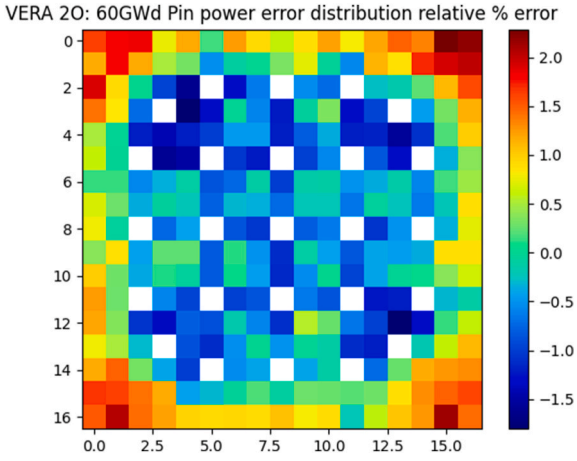


Fig. 26. Vera 2O: 60GWd/tHM pin power error distribution relative % error.

In the process of cross-section generation, the issue of missing flux tally in the low-energy thermal group when using a single pin model is encountered. To address this issue, several methods are considered. One approach involves using mixtures of fuel and moderator with different thicknesses to obtain flux values for the energy group without statistical data. By varying the thicknesses, the flux distribution across the energy range of interest can be captured. Another method is to set the flux value for the missing energy group to zero. This assumption assumes that the flux in that energy range is negligible or non-existent. Alternatively, an extrapolation technique can be employed, where the flux for the missing group is estimated based on statistical data from neighboring energy groups. This extrapolation relies on the assumption of a smooth flux distribution among adjacent energy ranges. The first method was chosen for this study.

4. Numerical verification

This section provides a case study to validate the two-stage approach

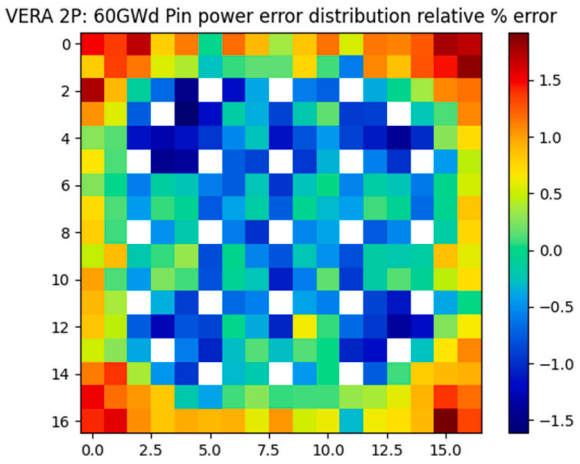


Fig. 27. Vera 2P: 60GWd/tHM pin power error distribution relative % error.

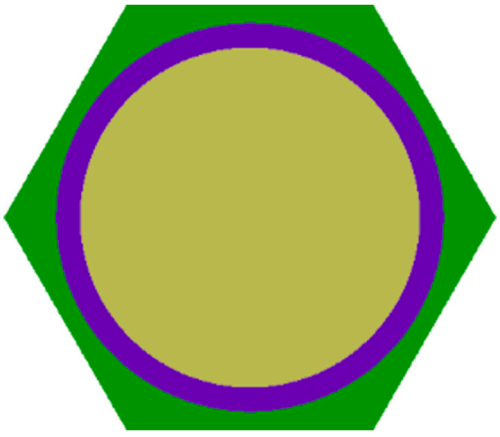


Fig. 28. The structure of the square pin-cell problem.

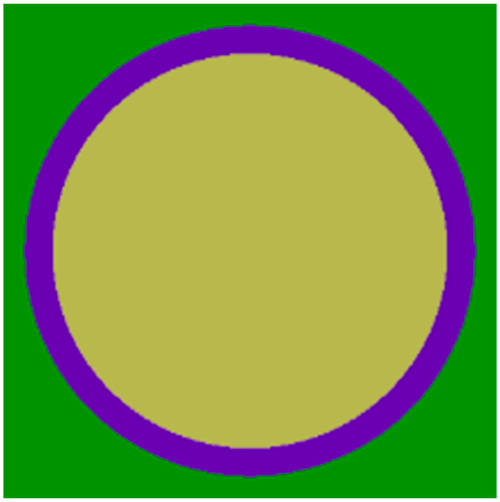


Fig. 29. The structure of the hexagonal pin-cell problem.

OpenMC/CRANE. The fuel pin and assembly models based on the pressurized water reactor (PWR) VERA benchmark, and the results by OpenMC/CRANE are given in section 4.1. Section 4.2 focus on the single fuel pin, fuel assembly and whole-core benchmark problems for fast reactors and present the detailed results.

Table 3
OpenMC/CRANE results for the pin-cell problem.

	OpenMC K_{eff}	OpenMC/CRANE K_{eff}	diff (pcm)
square pin	1.156	1.156	−14.9
hexagonal pin	1.172	1.172	−24.8

Table 4
Sub-assembly geometrical data.

Parameter	Unit	Operating state
Subassembly pitch	cm	21.2205
Subassembly duct outer flat-to-flat distance	cm	20.7468
Subassembly duct wall thickness	cm	0.4525
Number of fuel pins	cm	271
Outer radius of cladding	cm	0.5419
Inner radius of cladding	cm	0.4893
Fuel slug radius	cm	0.4742

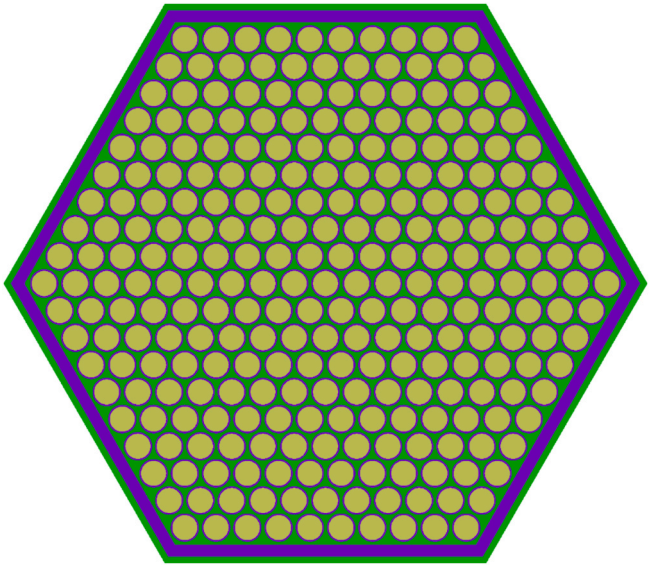


Fig. 30. Subassembly radial layout generated by OpenMC.

Table 5
Time-steps used for 2D fuel assembly depletion calculations.

	Time steps (EFPD)
OpenMC fuel single pin-cell model used to generate microscopic XS	102.5, 205, 307.5, 410
OpenMC reference assembly calculation	51.25, 102.5, 153.75, 205, 256.25, 307.5, 358.75, 410
OpenMC/CRANE assembly calculation	0.0, 25, 51.25, 75, 102.5, 125, 153.75, 175, 205, 225, 256.25, 275, 307.5, 325, 358.75, 375, 410

4.1. Verifications in PWR calculation

4.1.1. Verifications in PWR pin calculation

A single pin-cell calculation was conducted as a baseline. A VERA1B pin problem with 3.1 % w/o enrichment is selected, with the fuel, cladding, and moderator temperatures all set to 600 K and the moderator density specified at 0.7 g/cm^3. The geometry includes a fuel rod pitch of 1.26 cm, a cladding outer radius of 0.4750 cm, and a pellet radius of 0.4096 cm. The system operates at a power density of 40.0 W/gU. The geometry of the VERA 1B fuel pin is shown in Fig. 9.

Table 1 compares the resulting keff with the reference solution,

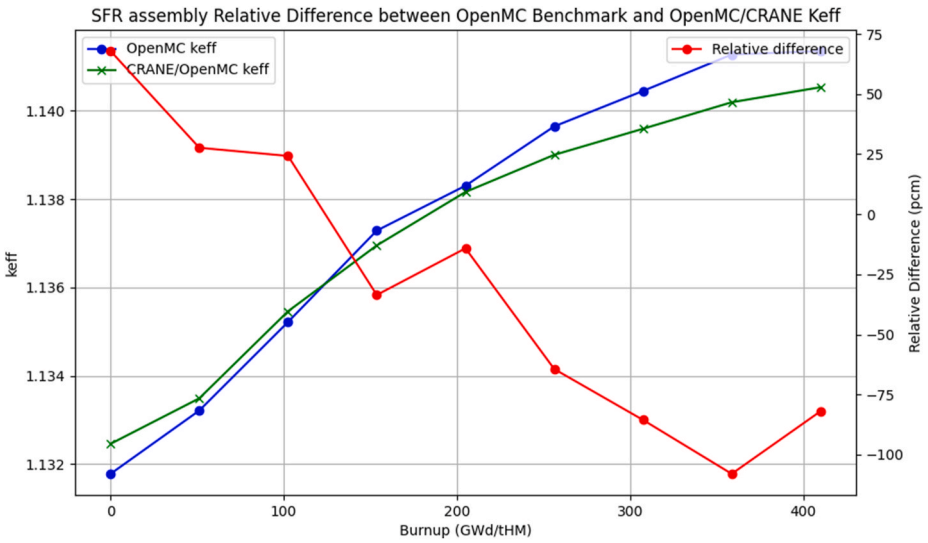


Fig. 31. SFR Assembly Relative Difference between OpenMC Benchmark and OpenMC/CRANE K_{eff} for 33 group.

Table 6
Comparison of Doppler reactivity between OpenMC reference and OpenMC/CRANE.

	OpenMC Ref	OpenMC/CRANE
Doppler constant (pcm/K)	−1.30	−1.35

Table 7
Comparison of Sodium void worth Between OpenMC Reference and OpenMC/CRANE.

	OpenMC Ref	OpenMC/CRANE
Sodium void worth (pcm)	2572.3	2480.5

showing a bias of around 169 pcm. Fig. 7 presents the flux spectrum, which reveals only minor deviations despite the observed reactivity difference. Although the overall spectral shape appears well maintained, additional work is required to clarify why a single-pin calculation exhibits this level of discrepancy. Because the current method employs scalar flux weighting in cross-section condensation and does not account for angle dependence, an inherent condensation error persists. While fine-mesh heterogeneous modeling partially mitigates the spatial and spectral coarsening typically introduced by condensation, it cannot entirely resolve angle-independent cross-section limitations. To reduce the discrepancy further, adopting angle-dependent total cross sections or introducing equivalence parameters may be necessary in future studies.

4.1.2. *Verifications in PWR assembly calculation*

The configurations of VERA2A and VERA2C benchmark can be seen

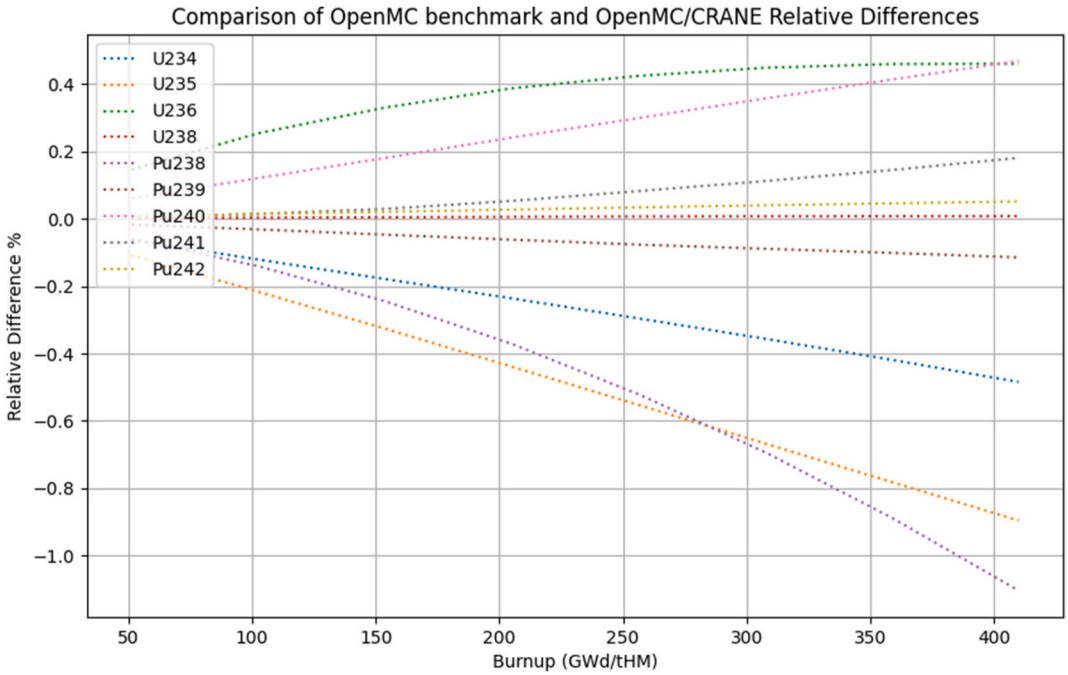


Fig. 32. Sfr assembly: Comparison of OpenMC and OpenMC/CRANE relative differences in atom densities of important nuclides.

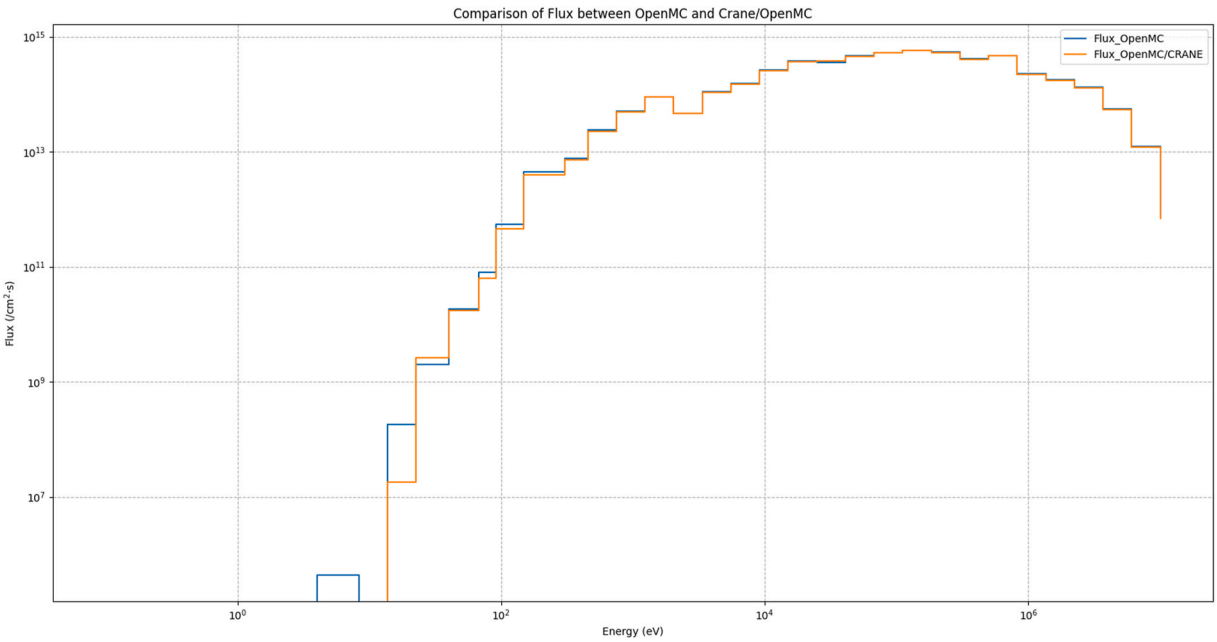


Fig. 33. Neutron spectrum of fuel assembly OpenMC Crane/OpenMC.

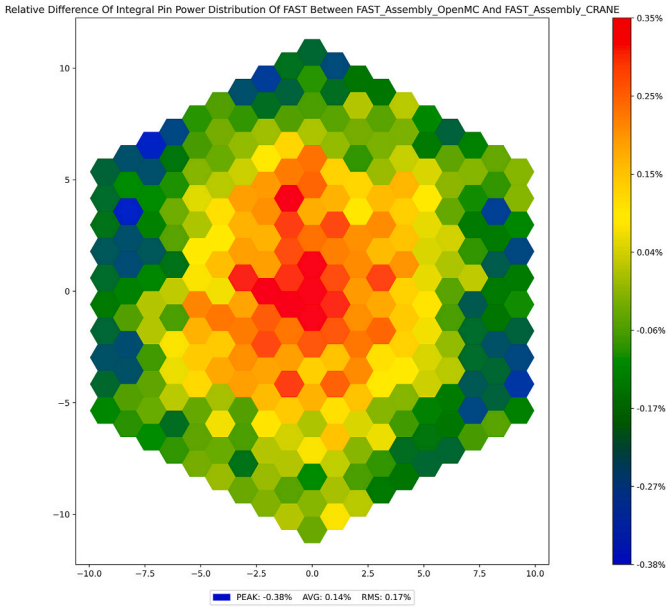


Fig. 34. Relative difference of integral pin power distribution between SFR assembly OpenMC/CRANE and OpenMC at 410 EPFD

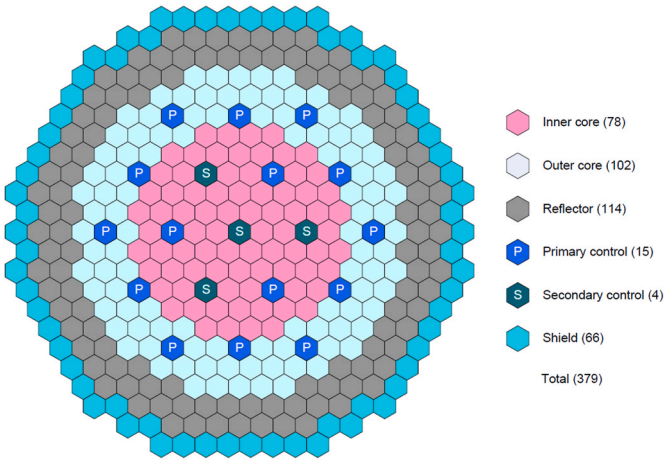


Fig. 35. Layout of MET-1000 full core.

in Fig. 8. The geometry of the VERA 2A and VERA 2C fuel pins is shown in Fig. 9. In these problems, the fuel rod pitch is 1.26 cm, the cladding outer radius is 0.4750 cm, and the pellet radius is 0.4096 cm. The power density is 40.0 W/gU. The fuel enrichment is 3.1 %, and the temperatures of the fuel, cladding, and moderator are set to 565 K. The moderator density is 0.743 g/cm^3.

VERA2C and VERA2A have different fuel and moderator temperatures. In the VERA2C case, the fuel temperature is 900K, and the moderator and cladding temperatures are 600K. The moderator density is 0.7 g/cm.

The benchmark provides detailed time steps up to 1500 effective full power days (EFPD). The CRANE and OpenMC reference solutions were computed using a detailed time step approach with 40 steps. For the generation of microscopic cross-section libraries in OpenMC, 11 steps were selected, as shown in Table 2.

Figs. 10 and 11 compare the absorption and fission cross sections of key isotopes between the target burnup step sizes (40 steps) and the coarse burnup step sizes (11 steps), calculated using the VERA1A single pin-cell model. The comparison demonstrates that the relative differences in the cross sections for the isotopes remain within 2 % between the two burnup step sizes. This indicates that using a coarser burnup step size of 11 steps does not adversely affect the accuracy of the generated cross sections.

To assess the influence of different energy group structures on reactivity, microscopic cross-section libraries were generated utilizing 25 and 69 energy groups, respectively. Calculations with these two energy group structures were then compared against the OpenMC reference results. Figs. 12 and 13 showcase the reactivity variation with burnup depth, corresponding to the two different energy group structures. It can be observed that reactivity is not highly sensitive to the variation in energy group structures. Therefore, the 25-group library can be used for calculations.

The relative error in the pin power distribution was analyzed using

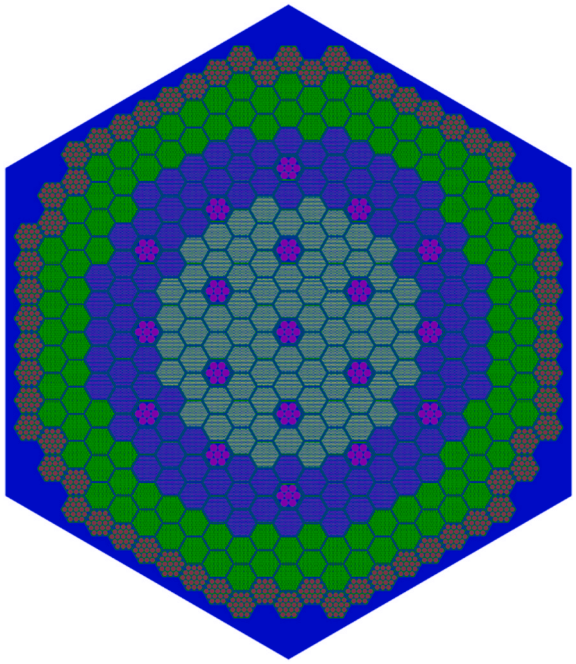


Fig. 36. Radial layout of the MET-1000 core generated by OpenMC.

Table 8
Main results between OpenMC and OpenMC/CRANE.

	OpenMC Ref	OpenMC/CRANE	Difference (pcm)
Multiplication factor at BOC	0.985324± 3.20408E-4	0.988755	343.1
Reactivity (pcm)	−1489.5	−1137.3	352.2
Doppler constant (pcm/K)	−0.28	−0.32	−0.04
Sodium void worth (pcm)	2887	2750	137

the 25-group library. Figs. 14 and 15 illustrate the calculated errors for the VERA2A and VERA2C benchmark cases, respectively. The analysis revealed that the power distribution calculations using the 25-group library exhibit reasonable accuracy, with limited deviations from the reference OpenMC results. These findings support the reliability and suitability of the 25-group library for accurately predicting the pin power distribution in both benchmark cases.

Furthermore, the variation of individual microscopic nuclide compositions over time was examined using the 25-group and 69-group microscopic cross-section libraries. Figs. 16 and 17 depict the trends in nuclide compositions for both libraries.

Then, the VERA 2G benchmark problem was selected to evaluate the performance of the super-cell approach in accurately modeling resonance effects. The configuration of the VERA 2G benchmark is shown in Fig. 18. The assembly features a fuel enrichment of 3.1 % and includes 24 Ag-In-Cd (AIC) control rods. The temperatures are set to 900 K for the

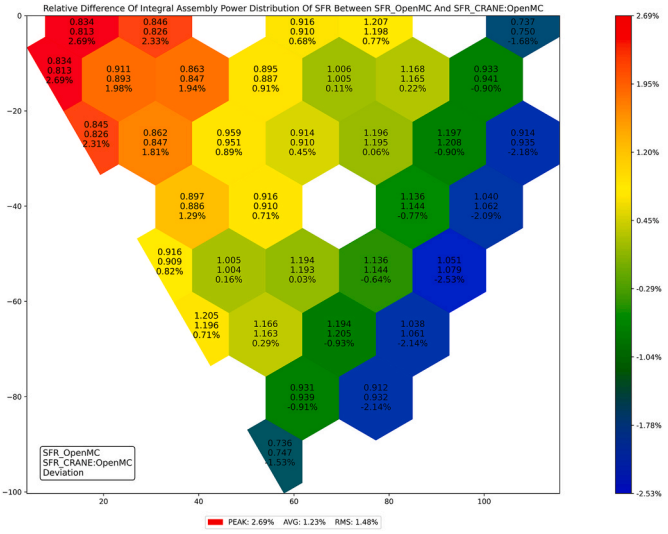


Fig. 38. Relative difference of integral assembly power distribution between SFR OpenMC/CRANE and OpenMC conclusion.

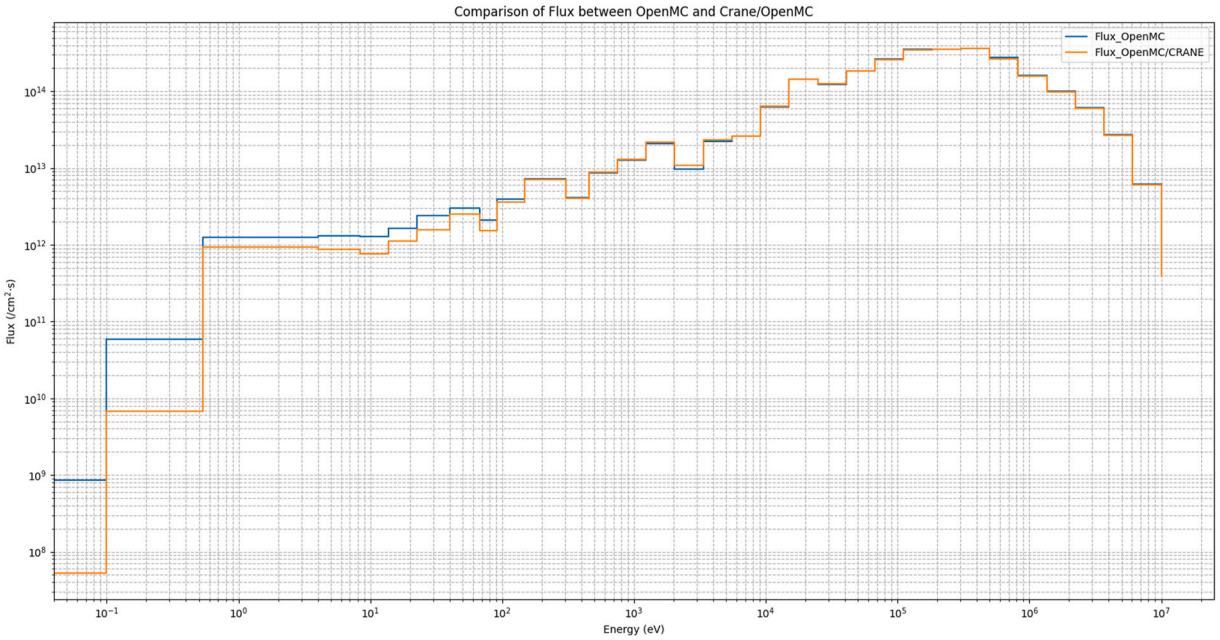


Fig. 37. Neutron spectrum of core OpenMC and OpenMC/CRANE.

fuel and 600 K for the AIC control rods, cladding, and moderator. The moderator density is specified as 0.700 g/cm^3.

To address the spatial self-shielding effects in this scenario, a nine-cell super-cell model—previously illustrated in Fig. 5—was employed, with the control rod positioned at the center and surrounded by eight fuel rods. Multigroup cross sections were generated using this super-cell configuration and compared against those derived from an exact assembly model. As shown in Fig. 19, the super-cell method effectively captures the resonance interactions between non-fuel and fuel regions. This capability is particularly important in thermal reactors, where materials such as Ag-109 in the AIC alloy exhibit strong low-energy resonance absorption. By providing a more precise treatment of spatial self-shielding, the super-cell model ensures reliable cross-section data for reactor analyses.

Next, the benchmark problems with Gd-bearing fuel assemblies are validated. The VERA 2O and 2P models, as illustrated in Figs. 20 and 21, share the same configuration as the 2C model but include gadolinium fuel rods. Specifically, model 2O features 12 gadolinium rods, while VERA 2P contains 24.

The cross-section generation model for fuel pins containing 5 % gadolinia oxide utilizes a detailed radial subdivision, dividing each pin into ten equal-volume regions. This stratified approach produces ten distinct cross-section datasets, effectively capturing spatial self-shielding effects in VERA 2O depletion calculations. The implementation of this discretization method is illustrated in Fig. 22.

In contrast to gadolinia-containing fuel pins, conventional non-gadolinia fuel pins are treated using a streamlined approach to maintain consistency with prior models. For these standard fuel pins, the cross section generation process adheres to the established single-pin model previously employed in VERA2A 2C calculations.

Furthermore, Fig. 23 compares the absorption cross sections generated by the single-pin model against those from the exact (assembly-level) configuration at the final burnup step. It specifically shows the difference in absorption cross sections for the primary absorbing isotopes Gd155 and Gd157 in a gadolinia pin subdivided into ten concentric rings. The relative errors for gadolinium in the outer rings are generally below 2 %, indicating high accuracy in these regions. However, gadolinium near the center of the pin exhibits higher statistical errors. Despite this, the overall error remains within reasonable limits.

The time-steps used for the VERA 2O and 2P assembly depletion calculations are the same as those in Table 2.

To assess the performance of the CRANE and OpenMC 25-group libraries, the K_{eff} and pin power distributions with burnup for the VERA 2O and VERA 2P models were compared. Figs. 24 and 25 show the K_{eff} variation with burnup for both benchmark. Figs. 26 and 27 illustrate the pin power distribution comparisons.

These analyses reveal that the reactivity and pin power distributions predicted by the 25-group microscopic cross-section library are consistent with the reference OpenMC results, demonstrating the library's suitability for the accurate neutronics simulation. The comparisons show that the 25-group library effectively captures the impact of gadolinium on reactivity and pin power distribution across different burnup steps. By validating the VERA 2O and VERA 2P models using CRANE and OpenMC, it is confirmed that the 25-group microscopic cross-section library is robust and reliable for simulations involving gadolinium-bearing fuel rods. An appropriate energy group structure can achieve higher computational efficiency while guaranteeing computational accuracy.

4.2. Verifications in SFR calculation

4.2.1. Verifications in SFR pin calculation

To validate the applicability of the methodology for fast reactors, the focus is first placed on the SFR pin calculation. Effective multiplication factor calculations are performed for the MOX-3600MWth single pin, as described in the OECD SFR benchmark report [25]. The pin-cell problem involves both square and hexagonal lattice configurations, as shown in Figs. 28 and 29. In this problem, the pin pitch is 1.1897 cm, while the radius of the MOX fuel region is 0.4742 cm. The EM10 cladding region has a radius of 0.5419 cm.

In the two-stage method, a 33-group energy structure is used to generate multigroup microscopic cross-section libraries for the fuel, cladding, and moderator separately. The effective multiplication factor by OpenMC and the two-stage method of OpenMC/CRANE are presented in Table 3. The preliminary results indicate that the two-stage method of OpenMC/CRANE closely matches the continuous-energy OpenMC calculations which provide preliminary verification of the feasibility of this approach at the single fuel assembly level in fast reactors.

4.2.2. Verifications in SFR assembly calculation

Upon completing the single fuel pin calculations, the analysis was extended to assembly-level calculations. The oxide fuel assembly model is detailed in the OECD SFR benchmark report [25], providing comprehensive information on the lattice input data for the SFR MOX3600MW oxide core. The lattice input data comes from one of the ten representative subassemblies of the SFR MOX3600MW oxide core at beginning of equilibrium cycle. The geometrical data for the subassembly can be found in Table 4, while the radial layout generated by OpenMC is illustrated in Fig. 30.

The two-stage method was applied to generate a 33-group microscopic cross-section library, followed by deterministic calculations. The time-steps used for the 2D fuel assembly depletion calculations are summarized in Table 5. This table shows the specific time-steps for generating microscopic cross sections using the OpenMC single fuel cell model, the OpenMC reference assembly calculations, and the OpenMC/CRANE assembly calculations.

Fig. 31 shows the relative difference in K_{eff} between the OpenMC benchmark and the OpenMC/CRANE results for the 33-group energy structure. As burnup progresses, reactivity increases due to favorable neutron balance for plutonium breeding. The relative differences, with a maximum of over 100 pcm, remain within acceptable limits throughout the burnup range, indicating the reliability of the coupled method.

The Doppler constant and sodium void worth are crucial for the safety analysis of fast reactors. The Doppler constant K_D is defined by:

$$K_D = \frac{\rho_{temperature} - \rho_{nominal}}{\ln \frac{T_{temperature}}{T_{nominal}}} \tag{19}$$

In this case, Doppler reactivity was calculated by changing the fuel temperature from the nominal value 1500 K–750 K. The Doppler effect comparison is presented in Table 6. The OpenMC/CRANE result shows forty pcm deviation in the Doppler constant.

The sodium void worth, $\Delta\rho$, is defined by the reactivity difference between the sodium voided and normal states:

$$\Delta\rho = \rho_{void} - \rho_{nominal} \tag{20}$$

where the subscripts void and nominal indicate the sodium voided and nominal states, respectively. Sodium void reactivity was calculated by changing the Na-23 density from the nominal value to 1 %.

The sodium void worth calculated in this work are summarized in Table 7. The results from OpenMC/CRANE underestimated by 92 pcm compared to OpenMC.

Fig. 32 compares the relative differences in atom densities of key nuclides (U-238, U-235, U-236, U-234, and various plutonium isotopes) between the OpenMC benchmark and OpenMC/CRANE results. The comparison shows good agreement, indicating that the coupled method accurately captures the isotopic evolution during burnup. Fig. 33 shows neutron spectrum of fuel assembly model.

Furthermore, Fig. 34 illustrates the relative differences in integral

pin power distribution between OpenMC/CRANE and the OpenMC reference at 410 EFPD.

4.2.3. Verifications in SFR core 2D calculation

The MET-1000 numerical benchmark, derived from the OECD SFR benchmark report [25], consists of a core with 72 internal fuel assemblies, 102 external fuel assemblies, 114 reflector components, 66 radial shielding components, and 19 control rod components. The benchmark utilizes two independent safety-grade reactivity control subsystems. The nominal power of the core is 1000 MWth, and the average fuel temperature and core structural temperature are 534.0 and 432.5 °C, respectively.

Fig. 35 illustrates the radial core layout of the MET-1000 core. Fig. 36 shows the OpenMC modeling of this core.

The detailed models and parameters used to generate the multigroup microscopic cross-section libraries are listed in the appendix.

Table 8 presents a comparison of key neutronic parameters calculated using the OpenMC and OpenMC/CRANE methodologies for the MET-1000 core benchmark. The parameters compared include the multiplication factor at the beginning of cycle (BOC), overall reactivity, Doppler constant, and sodium void worth.

When calculating the Doppler constant, the OECD/NEA MET-1000 benchmark was referred to, where the high fuel temperature is 1614 K. The OpenMC/CRANE result shows a deviation of 40 pcm in the Doppler constant. For calculating the sodium void worth, the same method used in the assembly calculations was employed, adjusting the Na-23 density from the nominal value to 1 % in the active core. The results from OpenMC/CRANE underestimated by 92 pcm compared to OpenMC.

The neutron spectrum results for the core, comparing OpenMC and OpenMC/CRANE, are shown in Fig. 37, with minimal deviations observed. Flux spectrum is normalized per unit lethargy.

The assembly power distribution for one-sixth of the core is shown in Fig. 38, with a maximum deviation of 2.69 % compared to OpenMC.

The discrepancy of 343 pcm in the keff is consistent with the tilt of the power distribution.

Due to the larger neutron mean free path and the anisotropy effects in fast reactors, the 33-group cross sections derived from a single pin-cell or super-cell model cannot adequately account for the core-wide spectral transition. Furthermore, the anisotropic scattering matrix is commonly weighted by the scalar flux spectrum, rather than by higher-order flux moments, which remains a major challenge in Monte Carlo-based cross-section generation for fast reactors (C. S. Lin and W. S. Yang, 2020). The impact of the energy group number and group structure, including these anisotropy considerations, will be investigated in subsequent work.

5. Conclusion

This study presents a methodology for generating heterogeneous multigroup microscopic cross-section libraries using OpenMC for three-dimensional neutron transport calculations, combined with CRANE for deterministic simulations. The proposed approach effectively captures the reactivity, isotopic evolution, and power distribution, as validated by preliminary 2D benchmark problems involving PWR and fast reactor models.

Future work will focus on extending the verification to full 3D core simulations to further verify the accuracy and robustness of the method. Additionally, enhancements in the coupling scheme between OpenMC and CRANE will be explored to improve computational efficiency and scalability. Further research will also include the application of this methodology to a broader range of advanced reactor designs, ensuring its adaptability and effectiveness in various nuclear reactor simulations.

CRediT authorship contribution statement

Bowen Cui: Writing – review & editing, Writing – original draft, Visualization, Validation, Software, Resources, Methodology, Investigation, Formal analysis, Conceptualization. **Guohua Chen:** Supervision, Software, Methodology, Investigation, Conceptualization. **Xiaofeng Jiang:** Writing – review & editing, Supervision, Methodology, Investigation, Formal analysis, Conceptualization.

Declaration of competing interest

The authors declare that they have no known competing financial interests or personal relationships that could have appeared to influence the work reported in this paper.

Acknowledgments

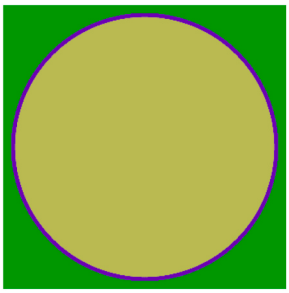
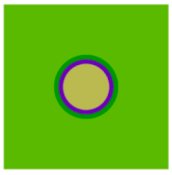
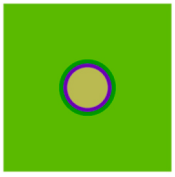
The author would like to thank Shanghai NuStar Nuclear Power Technology for its support to this work.

Appendix. Detailed Parameters and Models for Generating MGXS for 1000 MWth core

OpenMC Pin Cell Model		Generated MGXS	Specific model parameters
Fuel_inner		*Fuel_inner* *Inner_fuel_HT9* *Coolant*	Fuel or = 0.3236 cm Clad or = 0.38567 cm Cell pitch = 0.8966 cm (Filled with coolant) Fuel temperature = 807.15 k Clad temperature = 705.65 k Coolant temperature = 705.65 k
Fuel_outer		*Fuel_outer* *Outer_fuel_HT9*	Fuel or = 0.3236 cm Clad or = 0.38567 cm Cell pitch = 0.8966 cm (Filled with coolant) Fuel temperature = 807.15 k

(*continued on next page*)

(*continued*)

	OpenMC Pin Cell Model	Generated MGXS	Specific model parameters
Primary_control		*Primary_control_HT9* *Primary_contral_enriched_B4C*	Clad temperature = 705.65 k Coolant temperature = 705.65 k B4C or = 2.289005 cm Clad or = 2.36063 cm Cell pitch = 19.38284342 cm (Filled with mixed fuel and sodium) B4C temperature = 705.65 k Clad temperature = 705.65 k Homo temperature = 705.65 k
Reflector		*Reflector_HT9*	Fuel or = 0.3236 cm Clad or = 0.38567 cm Cell pitch = 2.31579028 cm (Filled with reflector_HT9) Fuel temperature = 807.15 k Clad temperature = 705.65 k Coolant temperature = 705.65 k Reflector temperature = 705.65 k
Shield		*Natural_B4C* *Shield_HT9*	Fuel or = 0.3236 cm Clad or = 0.38567 cm Coolant or = 0.4483 cm Cell pitch = 2.67840211 cm (Filled with natural B4C) Fuel temperature = 807.15 k Clad temperature = 705.65 k Coolant temperature = 705.65 k B4C temperature = 705.65 k

References

[1] E. Fridman, J. Leppänen, On the use of the Serpent Monte Carlo code for few-group cross section generation, Ann. Nucl. Energy 38 (2011) 1399–1405, https://doi.org/10.1016/j.anucene.2011.01.032.

[2] H.G.J. Ho Jin Park, Jin Shim Hyung, C.H. Kim, Generation of few-group diffusion theory constants by Monte Carlo code McCARD, Nucl. Sci. Eng. 172 (2012) 66–77, https://doi.org/10.13182/NSE11-22.

[3] J.E. Hoogenboom, V.A. Khotylev, J.M. Tholammakkil, Generation of Multi-Group Cross Sections and Scattering Matrices with the Monte Carlo Code MCNP5, American Nuclear Society - ANS, United States, 2007.

[4] B.F. William Boyd, Nelson Adam, Paul K. Romano, Samuel Shaner, K. Smith, Multigroup cross-section generation with the OpenMC Monte Carlo particle transport code, Nucl. Technol. 205 (2019) 928–944, https://doi.org/10.1080/00295450.2019.1571828.

[5] T.D.C. Nguyen, H. Lee, D. Lee, Use of Monte Carlo code MCS for multigroup cross section generation for fast reactor analysis, Nucl. Eng. Technol. 53 (2021) 2788–2802, https://doi.org/10.1016/j.net.2021.03.005.

[6] C.-S. Lin, W.S. Yang, An assessment of the applicability of multigroup cross sections generated with Monte Carlo method for fast reactor analysis, Nucl. Eng. Technol. 52 (2020) 2733–2742, https://doi.org/10.1016/j.net.2020.05.029.

[7] C.S. Lin, W.S. Yang, An assessment of the applicability of multigroup cross sections generated with Monte Carlo method for fast reactor analysis, Nucl. Eng. Technol. 52 (12) (2020) 2733–2742.

[8] Y. Wu, Q. Song, R. Wang, Y. Xiao, H. Gu, H. Guo, Development and verification of a Monte Carlo two-step method for lead-based fast reactor neutronics analysis, Nucl. Eng. Technol. 55 (2023) 2112–2124, https://doi.org/10.1016/j.net.2023.03.006.

[9] T.Q. Tran, A. Cherezov, X. Du, D. Lee, Verification of a two-step code system MCS/RAST-F to fast reactor core analysis, Nucl. Eng. Technol. 54 (2022) 1789–1803, https://doi.org/10.1016/j.net.2021.10.038.

[10] T.D.C. Nguyen, D. Lee, Group constants generation by Monte Carlo code MCS for LWR analysis, Comput. Phys. Commun. 285 (2023) 108642, https://doi.org/10.1016/j.cpc.2022.108642.

[11] T.M. Pandya, F. Bostelmann, M. Jessee, J. Ortensi, Two-step neutronics calculations with Shift and Griffin for advanced reactor systems, Ann. Nucl. Energy 173 (2022) 109131, https://doi.org/10.1016/j.anucene.2022.109131.

[12] J. Wang, Z. Li, M. Ding, Generation method and verification of pebble type VHTR multigroup cross sections based on OpenMC, Ann. Nucl. Energy 159 (2021) 108316, https://doi.org/10.1016/j.anucene.2021.108316.

[13] H. Park, H.G. Joo, Practical resolution of angle dependency of multigroup resonance cross sections using parametrized spectral superhomogenization factors, Nucl. Eng. Technol. 49 (6) (2017) 1287–1300.

[14] G. Giudicelli, K. Smith, B. Forget, Generalized equivalence methods for 3D multi-group neutron transport, Ann. Nucl. Energy 112 (2018) 9–16.

[15] P.K. Romano, N.E. Horelik, B.R. Herman, A.G. Nelson, B. Forget, K. Smith, OpenMC: a state-of-the-art Monte Carlo code for research and development, Ann. Nucl. Energy 82 (2015) 90–97, https://doi.org/10.1016/j.anucene.2014.07.048.

[16] K.S. Kim, Specification for the VERA depletion benchmark suite. https://doi.org/10.2172/1256820, 2015.

[17] Guohua, C., Chao, C., Lulin, Y., Bowen, C., Xiaofeng, J., n.d. CRANE Documentation [WWW Document]. URL https://docs.nustarnuclear.com/crane/index.html (accessed 3.22.24).

[18] R. Macfarlane, D.W. Muir, R.M. Boicourt, A.C. Kahler III, J.L. Conlin, The NJOY Nuclear Data Processing System, Version 2016, United States, 2017, https://doi.org/10.2172/1338791.

[19] M.B. Chadwick, M. Herman, P. Obložinský, M.E. Dunn, Y. Danon, A.C. Kahler, D. L. Smith, B. Pritychenko, G. Arbanas, R. Arcilla, R. Brewer, D.A. Brown, R. Capote, A.D. Carlson, Y.S. Cho, H. Derrien, K. Guber, G.M. Hale, S. Hoblit, S. Holloway, T. D. Johnson, T. Kawano, B.C. Kiedrowski, H. Kim, S. Kunieda, N.M. Larson, L. Leal, J.P. Lestone, R.C. Little, E.A. McCutchan, R.E. MacFarlane, M. MacInnes, C.

M. Mattoon, R.D. McKnight, S.F. Mughabghab, G.P.A. Nobre, G. Palmiotti, A. Palumbo, M.T. Pigni, V.G. Pronyaev, R.O. Sayer, A.A. Sonzogni, N.C. Summers, P. Talou, I.J. Thompson, A. Trkov, R.L. Vogt, S.C. van der Marck, A. Wallner, M. C. White, D. Wiarda, P.G. Young, ENDF/B-VII.1 nuclear data for science and technology: cross sections, covariances, fission product yields and decay data, Nucl. Data Sheets 112 (2011) 2887–2996, https://doi.org/10.1016/j.nds.2011.11.002.

[20] A.J.M. Plompen, O. Cabellos, C. De Saint Jean, M. Fleming, A. Algora, M. Angelone, P. Archier, E. Bauge, O. Bersillon, A. Blokhin, F. Cantargi, A. Chebboubi, C. Diez, H. Duarte, E. Dupont, J. Dyrda, B. Erasmus, L. Fiorito, U. Fischer, D. Flammini, D. Foligno, M.R. Gilbert, J.R. Granada, W. Haeck, F.-J. Hambsch, P. Helgesson, S. Hilaire, I. Hill, M. Hursin, R. Ichou, R. Jacqmin, B. Jansky, C. Jouanne, M.A. Kellett, D.H. Kim, H.I. Kim, I. Kodeli, A.J. Koning, A. Yu Konobeyev, S. Kopecky, B. Kos, A. Krása, L.C. Leal, N. Leclaire, P. Leconte, Y. O. Lee, H. Leeb, O. Litaize, M. Majerle, J.I. Márquez Damián, F. Michel-Sendis, R. W. Mills, B. Morillon, G. Noguère, M. Pecchia, S. Pelloni, P. Pereslavtsev, R. J. Perry, D. Rochman, A. Röhrmoser, P. Romain, P. Romojaro, D. Roubtsov, P. Sauvan, P. Schillebeeckx, K.H. Schmidt, O. Serot, S. Simakov, I. Sirakov, H. Sjöstrand, A. Stankovskiy, J.C. Sublet, P. Tamagno, A. Trkov, S. van der Marck, F. Álvarez-Velarde, R. Villari, T.C. Ware, K. Yokoyama, G. Žerovnik, The joint evaluated fission and fusion nuclear data library, JEFF-3.3, Eur. Phys. J. A 56 (2020) 181, https://doi.org/10.1140/epja/s10050-020-00141-9. Art. Nr.

[21] A. Yamamoto, Evaluation of background cross section for heterogeneous and complicated geometry by the enhanced neutron current method, J. Nucl. Sci. Technol. 45 (12) (2008) 1287.

[22] G. Rimpault, Algorithmic Features of the ECCO Cell Code for Treating Heterogeneous Fast Reactor Subassemblies, 1995.

[23] J.R. Askew, F.J. Fayers, P.B. Kemshell, General description of the lattice code WIMS, J. Br. Nucl. Energy Soc. 5 (1966) 564–585. Oct 1966.

[24] J. Rhodes, K. Smith, D. Lee, CASMO-5 Development and Applications, 2006.

[25] N.E. Stauff, T.K. Kim, T.A. Taiwo, L. Buiron, G. Rimpault, E. Brun, Y.K. Lee, I. Pataki, A. Kereszturi, A. Tota, C. Parisi, E. Fridman, N. Guilliard, T. Kugo, K. Sugino, M.M. Uematsu, A. Ponomarev, N. Messaoudi, R. Lin Tan, T. Kozlowski, W. Bernnat, D. Blanchet, E. Brun, L. Buiron, E. Fridman, N. Guilliard, A. Kereszturi, T.K. Kim, T. Kozlowski, T. Kugo, Y.K. Lee, R. Lin Tan, N. Messaoudi, C. Parisi, I. Pataki, A. Ponomarev, G. Rimpault, N.E. Stauff, K. Sugino, T.A. Taiwo, A. Tota, M.M. Uematsu, S. Monti, A. Yamaji, Y. Nakahara, J. Gulliford, Benchmark for neutronic analysis of sodium-cooled fast reactor cores with various fuel types and core sizes. Nuclear Energy Agency of the OECD (NEA), 2016.